THE OHIO STATE UNIVERSITY

Curvature of Blended Rolled Edge Reflectors at the Shadow Boundary Contour

S.W. Ellingson

The Ohio State University

ElectroScience Laboratory

Department of Electrical Engineering
Columbus, Ohio 43212

Technical Report No. 716148-29
Grant No. NSG-1613
April 1988

National Aeronautics and Space Administration
Langley Research Center
Hampton, Virginia 23665

NOTICES

When Government drawings, specifications, or other data are used for any purpose other than in connection with a definitely related Government procurement operation, the United States Government thereby incurs no responsibility nor any obligation whatsoever, and the fact that the Government may have formulated, furnished, or in any way supplied the said drawings, specifications, or other data, is not to be regarded by implication or otherwise as in any manner licensing the holder or any other person or corporation, or conveying any rights or permission to manufacture, use, or sell any patented invention that may in any way be related thereto.

50272-101

REPORT DOCUMENTATION PAGE	1. REPORT NO.	2.	3. Recipient's Accession No.

4. Title and Subtitle

CURVATURE OF BLENDED ROLLED EDGE REFLECTORS AT THE SHADOW BOUNDARY CONTOUR

5. Report Date
April 1988

6.

7. Author(s)
S.W. Ellingson

8. Performing Organization Rept. No.
716148-29

9. Performing Organization Name and Address
The Ohio State University
ElectroScience Laboratory
1320 Kinnear Road
Columbus, Ohio 43212

10. Project/Task/Work Unit No.

11. Contract(C) or Grant(G) No.
(C)
(G) NSG-1613

12. Sponsoring Organization Name and Address
National Aeronautics and Space Administration
Langley Research Center
Hampton, Virginia 23665

13. Type of Report & Period Covered
Technical

14.

15. Supplementary Notes

16. Abstract (Limit: 200 words)

A technique is given to compute the radius of curvature of blended rolled edge reflector surfaces at the shadow boundary, in the plane perpendicular to the shadow boundary contour. This curvature must be known in order to compute the spurious endpoint contributions in the physical optics (PO) solution for the scattering from reflectors with rolled edges. The technique is applicable to reflectors with radially-defined rim-shapes and rolled edge terminations. The radius of curvature for several basic reflector systems is computed, and it is shown that this curvature can vary greatly along the shadow boundary contour. Finally, the total PO field in the target zone of a sample compact range system is computed and corrected using the shadow boundary radius of curvature, obtained using the technique. It is shown that the fields obtained are a better approximation to the true scattered fields.

17. Document Analysis a. Descriptors

b. Identifiers/Open-Ended Terms

c. COSATI Field/Group

18. Availability Statement	19. Security Class (This Report) Unclassified	21. No. of Pages 56
	20. Security Class (This Page) Unclassified	22. Price

(See ANSI-Z39.18) See Instructions on Reverse OPTIONAL FORM 272 (4-77) (Formerly NTIS-35) Department of Commerce

TABLE OF CONTENTS

LIST OF FIGURES

1 Introduction

The physical optics (PO) approximation is commonly used to determine the electromagnetic scattering from large structures. The PO technique is relatively well understood and is generally easy to implement. Unfortunately, the PO approximation assumes incorrect surface currents near edges and incident shadow boundaries. These incorrect currents lead to erroneous contributions such as the shadow boundary term associated with a curved surface [1]. This contribution is referred to as the *endpoint contribution* and the process of subtracting the endpoint contribution from the PO field in order to obtain a better approximation of the true scattered field is called the *endpoint correction*. Gupta and Burnside [1] have shown that in the specular region of a smooth conducting body the erroneous contribution has the form of an infinite series. In high frequency situations, the series can be approximated by the first two terms. In this report, the first and second terms are referred to as the *first-order* and *second-order* endpoint contributions, respectively. Gupta et. al. [2] have found an efficient numerical technique for evaluating these terms for arbitrarily shaped structures.

The second-order endpoint contribution requires the knowledge of the radius of curvature of the surface at the shadow boundary in a plane perpendicular to the shadow boundary contour. In this report, a numerical technique for finding this radius of curvature for compact range main reflectors is presented. This technique is applicable to reflectors which are designed according to the technique discussed by Pistorius [3]. Such reflectors have parabolic regions which have convex, rectangular, or concave rim-shapes. These reflectors have rolled edge terminations which may be elliptic or blended, and are radially attached. The reflectors may be center- or offset-fed. Using this technique, the radius of curvature is calculated along the shadow boundaries of various reflector systems. Examples of reflectors having circular, square, and concave rim-shapes are analyzed for both center- and offset-fed configurations. It is shown that, in general, the radius of curvature varies along the shadow boundary contour. The variation for offset-fed systems is greater than that for center-fed systems. Furthermore, the magnitude of the radius of curvature generally increases with increasing height and offset.

In order to better understand the significance of the second-order endpoint contributions, the scattered fields of a representative compact range reflector system are computed. The system has an offset-fed main reflector with a concave rim-shape and blended rolled edges. It is fed by a Gregorian subreflector feed system. In the analysis, the PO fields are calculated at various locations in the target zone. The effects of first- and second-order endpoint correction are then demonstrated. It is shown that the PO fields after first- and second-order correction are much closer to the expected scattered fields.

The remainder of this report is organized as follows. In Section 2, the technique used to specify rolled-edge surfaces [3] is outlined. In Section 3, the technique for finding the radius of curvature needed for second-order endpoint correction is presented. In Section 4, this technique is demonstrated for a variety of reflector systems. In Section 5, the scattered fields of an offset-fed reflector system are computed. The total calculated PO field as well as the fields after first- and second-order endpoint correction are compared. It is shown that the PO field after first- & second-order endpoint correction is a better approximation of the true scattered field. Section 6 contains conclusions.

2 Main Reflector Geometry

Rolled edges are added to the parabolic reflecting surface of compact range main reflectors in order to reduce rim diffraction into the target zone. A rolled edge works by reducing the physical discontinuity at the edges and by redirecting "stray" energy out of the target zone, as shown in Fig. 1.

Rolled edges can be generated by attaching a section of an ellipse to each point on the rim of the parabolic surface. Since this section need not nessessarily be a regular ellipse, it is referred to as the *rolled edge contour* in this report. The alignment of the rolled edge contour is such that the combined surfaces are continuous at the junction (see Fig. 2). A variety of techniques exist for adding the elliptic sections (see Fig. 3). The "intuitive" approach is shown in Fig. 3a. One adds the elliptic sections in the plane perpendicular to the tangent to the rim of the parabolic surface (*perpendicular* attachment). This technique has several shortcomings,

however. First, it is not obvious how one should add the rolled edge at corners of the parabolic surface. Simply "pivoting" the rolled edge around the corner leads to field caustics which may limit the usable target zone. Another disadvantage of this technique is limited flexibility in the choice of the rim-shape. Using perpendicular attachment for reflectors with concave rim-shapes, for example, may lead to multiple definitions of the rolled edge surface, as shown in Fig. 4. An alternate technique for adding the rolled edge, *radial* attachment, is illustrated in Fig. 3b. This method involves attaching the rolled edge contours in planes extending radially outward from the center of the reflector. Specifically, the rolled edge contour is added in the plane coincident with $\hat{\mathbf{n}}$, where $\hat{\mathbf{n}}$ is the surface unit normal to the parabolic region at the junction point, as shown in Fig. 2. Reflectors having rim-shapes which can be expressed as a single-valued radial function are easily dealt with using this technique, concave rims included. The caustic problem mentioned above is avoided using this technique. The drawback of radial attachment is simply that rolled edges are not attached in the optimum (i.e. perpendicular) direction. All reflectors considered in this report have radially-attached rolled edges.

In general, rolled edges may be *elliptic* or *blended*. Blended rolled edges result from a blending between an extension of the parabolic surface and a simple ellipse. The goal of blending is to make the junction as smooth as possible. This involves eliminating the discontinuity in the radius of curvature and its first few derivatives at the junction. A blending function which makes the first $n-1$ derivatives of the radius of curvature continuous is called an *n^{th}-order blending function*.

In this report it is assumed that the same rolled edge contour is used at every junction point; however, it is a simple matter to extend the techniques discussed below to cover situations where the rolled edge contour is variable with respect to the junction point. The technique used at Ohio State to define and generate rolled edge surfaces is outlined below:

1. A cartesian coordinate system is established. This establishes *main* or *global* coordinates.

2. The parabolic region of the main reflector is generated (see Fig. 5). First, a defining paraboloid is established having the following equa-

tion:

$$z = \frac{x^2 + y^2}{4f_c}$$

where f_c is the focal length of the main reflector. Then the *junction contour* is established to be the desired outline of the parabolic surface of the main reflector. The junction contour may be circular, rectangular, or convex. The focus of the system is established at $(x, y, z) = (0, 0, f_c)$. The focus may be either a feed location (focus-fed systems) or a caustic (e.g. systems using Gregorian subreflector feed systems). Rays reflected from the parabolic region travel in the $+z$ direction.

3. At each point along the junction contour, a local 2-dimensional cartesian coordinate system is defined. Its axes, $\hat{\mathbf{x}}_e$ and $\hat{\mathbf{y}}_e$, are determined as follows:

   - First $\hat{\mathbf{n}}$, the surface unit normal to the parabolic surface at the junction contour, is found. Of the two possibilities, $\hat{\mathbf{n}}$ is selected to be the normal which is most nearly pointing towards the focus. Then $\hat{\mathbf{y}}_e$ is defined by

     $$\hat{\mathbf{y}}_e = -\hat{\mathbf{n}}$$

   - Next, a vector $\hat{\mathbf{p}}$ is found as follows (see Fig. 6). Given the junction point J and the center of the reflector, O, one finds the projections J' and O' of J and O in the xy plane. Then, one finds the radial line R which connects J' and O'. $\hat{\mathbf{p}}$ is defined to be perpendicular to R and also in the xy plane. Of the two possibilities, $\hat{\mathbf{p}}$ is chosen such that $\hat{\mathbf{y}}_e \times \hat{\mathbf{p}}$ is directed away from parabolic region. It can be shown that

     $$\hat{\mathbf{p}} = p_1\hat{\mathbf{x}} + p_2\hat{\mathbf{y}}$$

     where

     $$p_1 = \frac{-(y_j - y_{ave})}{\sqrt{x_j^2 + (y_j - y_{ave})^2}}$$

     $$p_2 = \frac{x_j}{\sqrt{x_j^2 + (y_j - y_{ave})^2}}$$

- Finally, $\hat{\mathbf{x}}_e$ is defined by

$$\hat{\mathbf{x}}_e = \frac{\hat{\mathbf{y}}_e \times \hat{\mathbf{p}}}{|\hat{\mathbf{y}}_e \times \hat{\mathbf{p}}|}$$

4. A rolled edge contour is determined at each point along the junction contour. The contour has the form of an analytic function, $\mathbf{r}(\gamma)$, in main coordinates. γ is the angle parameter shown in Fig. 2. In general, $\mathbf{r}(\gamma)$ has the form:

$$\mathbf{r}(\gamma) = b(\gamma)\mathbf{r}_{ellipse}(\gamma) + (1 - b(\gamma))\mathbf{r}_{parabola}(\gamma)$$

where $\mathbf{r}(\gamma)$, $\mathbf{r}_{ellipse}(\gamma)$, and $\mathbf{r}_{parabola}(\gamma)$ are all expressed in main coordinates (see Fig. 7). $\mathbf{r}_{ellipse}(\gamma)$ is the parametric equation for an ellipse in main coordinates. In local $(\hat{\mathbf{x}}_e\hat{\mathbf{y}}_e)$ coordinates, this is expressed as:

$$\mathbf{r}^e_{ellipse}(\gamma) = \hat{\mathbf{x}}_e a_e sin\gamma + \hat{\mathbf{y}}_e b_e(1 - cos\gamma)$$

The general transformation from local to main coordinates is given by:

$$\begin{pmatrix} x(\gamma) \\ y(\gamma) \\ z(\gamma) \end{pmatrix} = \begin{pmatrix} x_{p1} & y_{p1} \\ x_{p2} & y_{p2} \\ x_{p3} & y_{p3} \end{pmatrix} \begin{pmatrix} x_e(\gamma) \\ y_e(\gamma) \end{pmatrix} + \begin{pmatrix} x_j \\ y_j \\ z_j \end{pmatrix}$$

where (x_j, y_j, z_j) are the coordinates of the junction point (main coordinates). The *direction cosines* are given by

$$\begin{aligned}
y_{p1} &= \frac{x_j}{\sqrt{x_j^2 + y_j^2 + 4f_c^2}} \\
y_{p2} &= \frac{y_j}{\sqrt{x_j^2 + y_j^2 + 4f_c^2}} \\
y_{p3} &= \frac{-2f_c}{\sqrt{x_j^2 + y_j^2 + 4f_c^2}} \\
x_{p1} &= \frac{-y_{p3}p_2}{y_{pg}} \\
x_{p2} &= \frac{y_{p3}p_1}{y_{pg}} \\
x_{p3} &= \frac{y_{p1}p_2 - y_{p2}p_1}{y_{pg}}
\end{aligned}$$

where

$$y_{pg} = \sqrt{(y_{p3}p_2)^2 + (y_{p3}p_1)^2 + (y_{p1}p_2 - y_{p2}p_1)^2}.$$

The parametric equation of an extention of a parabolic surface contour from the junction point is defined by $\mathbf{r}_{parabola}(\gamma)$. In main coordinates:

$$\begin{aligned} x_{parabola}(\gamma) &= \gamma(\frac{x_m}{\gamma_m})x_{p1} + x_j \\ y_{parabola}(\gamma) &= \gamma(\frac{x_m}{\gamma_m})x_{p2} + y_j \\ z_{parabola}(\gamma) &= \frac{x^2_{parabola} + y^2_{parabola}}{4f_c} \end{aligned}$$

where x_m is a blending parameter which controls the length of the extension of the parabolic contour from the junction point to be used in blending. The maximum extent of the rolled edge is specified by γ_m, as shown in Fig. 7.

Finally, $b(\gamma)$ is a blending function. As discussed above, a variety of functions are possible, but they all must have the property $0 \leq b(\gamma) \leq 1$ on the interval $0 \leq \gamma \leq \gamma_m$. In the special case of elliptic rolled edges, $b(\gamma) = 1$; i.e., the rolled edge contour is a pure ellipse.

All of the rolled edge contours taken together define the rolled edge surface.

Having defined the geometry of the rolled edges, we now face the problem of determining how these surfaces affect endpoint contributions. Gupta and Burnside have shown ([1],[2]) that the curvature in the surface of a perfectly conducting body at the shadow boundary contour must be known in order to determine the second- and higher-order endpoint contributions. Specifically, one must know the radius of curvature at the endpoint in the plane perpendicular to the shadow boundary contour. This radius of curvature is designated "a" in this report. For all but very simple compact range configurations (e.g. center-fed circular main reflectors), finding "a" exactly is a difficult task. The reason is that the rolled edge surfaces considered here generally cannot be expressed as a single analytic equation. A numerical technique for calculating "a" for reflectors with radially-attached rolled edges is presented below.

3 Computing the Shadow Boundary Radius of Curvature

As shown in Fig. 8, "a" is the radius of curvature of the rolled edge surface at the shadow boundary in the plane perpendicular to the shadow boundary contour. In Fig. 8, P is the endpoint of interest, C is the shadow boundary contour, $\hat{\mathbf{e}}$ is the unit tangent to C at P, and S is the plane perpendicular to $\hat{\mathbf{e}}$ at P. Given C and P, the idea is to find two points P_1 and P_2 close to P which are simultaneously on the rolled edge surface and in the plane S. Since any three points define a circle, three points very close together on a surface define a circle whose radius is approximately equal to the local radius of curvature in the plane defined by the points. In light of this, the problem is now to find suitable points P_1 and P_2. For some cases this is quite difficult: the reason is that $\mathbf{r}(\gamma)$ may not lie in S (see Fig. 9). Thus, P_1 and P_2 may lie on radial contours other than $\mathbf{r}_P(\gamma)$. Since the procedure for finding each of these points is the same, the outline below only discusses how to find P_1.

1. Determine $\hat{\mathbf{e}}$. Note $\hat{\mathbf{e}}$ is approximately the difference between the coordinates of P and those of a nearby point on the shadow boundary. For this technique, the direction of $\hat{\mathbf{e}}$ is unimportant.

2. Identify S. Note that the locus of points in S is given by

$$\hat{\mathbf{e}} \cdot (\mathbf{r}_S - \mathbf{P}) = 0$$

   where $\mathbf{P}$ is the location of P in global coordinates, and $\mathbf{r}_S$ is any point in S.

3. Find $\mathbf{r}_P(\gamma_C + \Delta\gamma)$. Here γ_C is given by

$$\mathbf{r}_P(\gamma_C) = \mathbf{P}$$

   and $\Delta\gamma$ is approximately the difference angle from P to P_1.

4. Determine if $\mathbf{r}_P(\gamma)$ lies entirely in S. Since $\mathbf{r}_P(\gamma)$ lies in the plane defined by $\hat{\mathbf{x}}_e$ and $\hat{\mathbf{y}}_e$, $\mathbf{r}_P(\gamma)$ and S are coincident if both $\hat{\mathbf{x}}_e$ and $\hat{\mathbf{y}}_e$ are perpendicular to $\hat{\mathbf{e}}$; i.e. if

$$\hat{\mathbf{x}}_e \cdot \hat{\mathbf{e}} = \hat{\mathbf{y}}_e \cdot \hat{\mathbf{e}} = 0$$

If $\mathbf{r}_P(\gamma)$ lies in S, then $\mathbf{P_1}$ is simply $\mathbf{r}_P(\gamma_C + \Delta\gamma)$. Otherwise, $\mathbf{r}_P(\gamma_C + \Delta\gamma)$ will serve as an initial estimate of a good value for $\mathbf{P_1}$.

5. Determine the distance between $\mathbf{r}_P(\gamma_C + \Delta\gamma)$ and S. This distance is given by

$$D = \hat{\mathbf{e}} \cdot (\mathbf{P_1} - \mathbf{P})$$

6. Determine a nearby rolled edge contour by locating a new junction contour point some small distance Δl from the current junction point along the junction contour. Let this new rolled edge contour be $\mathbf{r}_2(\gamma)$.

7. Let $\mathbf{r}_2(\gamma_C + \Delta\gamma)$ be the new candidate for $\mathbf{P}_1$.

8. Recalculate the distance D between P_1 and S.

9. If $|D|$ is within a predetermined error tolerance, then let $\mathbf{r}_2(\gamma_C + \Delta\gamma)$ be the final location of P_1. Otherwise, select yet another junction contour point by comparing the current and previous values of D, determining a new Δl, and then repeating steps 6-9 until $|D|$ falls within the specified tolerance.

Selecting $\mathbf{r}_P(\gamma_C - \Delta\gamma)$ instead of $\mathbf{r}_P(\gamma_C + \Delta\gamma)$ in step 3 is the only change that is required in order to use this algorithm to find P_2. Once P, P_1, and P_2 are all known they can be used to define a circle whose radius is approximately equal to the required radius of curvature, "a".

The parameter $\Delta\gamma$, which is proportional to the spacing between P, P_1, and P_2, must be chosen carefully in order to obtain accurate results. Clearly one should choose $\Delta\gamma$ as small as possible, thus letting the points be quite close together and improving the accuracy of the approximation. If $\Delta\gamma$ is *too* small however, the spacing between points will be so slight that even very small errors in coordinate values will lead to significant error in the calculated radius. For systems such as those discussed in this report, $\Delta\gamma = 1^o$ always seems to work well.

4 Shadow Boundary Radius of Curvature for Various Compact Range Reflectors

To demonstrate the technique presented above, "a" is calculated for six different reflector systems. The first system is a center-fed circular main reflector with a focal length $f_c = 8.0ft$ (see Fig. 10). The junction contour has a diameter of $10.0ft$. The reflector has elliptic rolled edge terminations with $a_e = 2.298ft$ and $b_e = 0.597ft$. This system is circularly symmetrical; thus, the plane S is *always* coincident with the rolled edge countour $\mathbf{r}(\gamma)$, and "a" has the same value at each point on the shadow boundary. This is seen in Fig. 11, in which "a" is calculated using the technique presented in Section 3. An additional test is available for deciding the validity of the results obtained: "a" can be determined exactly in the principal (yz) plane [3] and is found to be 0.224 ft, which agrees with the results of Fig. 11. In fact, the values found for "a" in the principal plane of all the systems examined here are in close agreement with the exact values.

Next a center-fed square reflector system (Fig. 12) is examined. This system is identical to the previous system, except that the reflector now has a square junction contour. The length of the sides of the junction contour for this reflector is equal to the diameter of the junction contour of the previous reflector. In this case, "a" is as shown in Fig. 13. As one might expect, "a" is symmetric about $x = 0$ and $y = 0$, and "a" in the principal plane is the same as that for system 1. The square reflector, however, has "a" increasing with $|x|$ along the horizontal sides and increasing with $|y|$ on the vertical sides. The maximum values of "a" occur at the corners.

A center-fed reflector with a concave junction contour (Fig. 14) is considered next. In this case, the junction contour is concave and symmetric about both x and y. The junction contours of all of the concave reflectors considered in this study were defined using the method discussed by Pistorius [3]. The minimum dimension of the junction contour is equal to the length of the sides of the junction contour in the previous case. Fig. 15 shows "a" along the shadow boundary of this reflector. Note that the variation in "a" is the same as that of the square reflector, except the magnitude of the variation is slightly greater. This is to be expected since the corners protrude further from the center than in the square-contour case.

Offset-fed reflectors are considered next. The system shown in Fig. 16 is an offset-fed reflector with a circular junction contour. Note that it is an offset-fed version of the circular reflector previously examined. The center of the reflector has been shifted from $y = 0$ to $y = 9.0ft$. The "a"-variation is shown in Fig. 17. In this case "a" is smoothly varying along the shadow boundary and "a" has a maximum at the shadow boundary point corresponding to the top of the reflector, and a minimum at the bottom. Note that "a" at the top of the reflector is greater than the principal plane value in the center fed-case ($a = 0.224ft$), while "a" at the bottom is less than this value. Thus, for an offset-fed circular reflector system, the variation in "a" is greater than that for the corresponding center-fed system.

The system shown in Fig. 18 is an offset-fed version of the center-fed square reflector considered above. The offset is once again $9.0ft$ in the $+y$-direction. The radius of curvature for this reflector is shown in Fig. 19. Note that the variation in "a" is again quite large. As in the case of the offset-fed circular reflector, The principal plane values differ from those of the center-fed case. Finally, note that the "a"-variation now has a jump discontinuity at the corners. This discontinuity is due to a corresponding discontinuity in the shadow boundary contour. This discontinuity appears when a corner of the reflector is above some minimum height. The extent of the discontinuity increases with increasing height.

The last system considered is shown in Fig. 20. It is an offset-fed version of the center-fed concave reflector of Fig. 14. Again, the offset is 9.0 ft in the $+y$-direction. Fig. 21 shows "a" along the shadow boundary of this reflector. Note that the variation in "a" is similar to that for the analogous square reflector case. Once again, the protruding corners of the concave shape lead to a larger variation in "a ".

From the above examples it is clear that the radius of curvature "a" for main reflectors with rolled edge terminations in general is not constant. The amount of variation in "a" is greater for offset-fed main reflectors. Furthermore, "a" tends to increase with increasing displacement between the endpoint and the z-axis. Thus, the assumption that "a" is constant along the shadow boundary contour will usually lead to incorrect second-order endpoint contributions. This conclusion will be reinforced by the results of Section 5, where the scattered fields in the target zone of a representative

compact range will be calculated. This compact range has an offset-fed main reflector (Fig. 22) with a focal length $f_c = 5.544ft$. It has a concave junction contour with minimum dimensions of $6.0ft \times 4.588ft$ and is offset $6.5ft$ in the $+y$-direction; thus, it is smaller and has less offset than the previous concave reflector (Fig. 20). The rolled edge terminations have the same dimensions, $a_e = 2.298ft$ and $b_e = 0.597ft$; however in this case, the rolled edges will be blended. *Cosine-squared* blending is used with $x_m = 6.765feet$. Cosine-squared blending ensures that the surface, as well as the first three derivatives of the radius of curvature, will all be continuous at the junction point.

Fig. 23 shows "a" along the shadow boundary contour of this reflector. Note that the variation is quite small relative to the variation seen in Fig. 21. This is due to the smaller size and offset of this reflector.

The scattered fields in the target zone of this system are computed next.

5 PO Endpoint Correction

In this section, the scattered fields in the target zone of the compact range system shown in Fig. 22 are computed. Field patterns are calculated along four different *cuts* in the target zone. These cuts are illustrated in Fig. 24. All of the cuts lie entirely in the plane $z = 15.0ft$, which is approximately $13.1ft$ from the center of the main reflector. For this study, a Gregorian subreflector feed system, as discussed in [3], is used. A schematic of the system is shown in Fig. 25. The specifications of the subreflector feed are $a_{sr} = 5.25feet$, $b_{sr} = 4.308feet$, $\beta_{sr} = 5.5°$, and $\alpha = 20.0°$. The subreflector is fed by vertically-polarized Huygens source operating at 2.0 GHz.

- **Principal Plane Cut**

  The first cut considered is in the principal (yz) plane. Fig. 26a shows the calculated total PO field along the cut, as well as the geometrical optics (GO) field. Note that the PO field is offset from the GO field and has strong, rapid oscillations. The difference between the PO and GO fields is due to the erroneous endpoint contributions plus legitimate higher-order scattered fields. The dominant contribution to the higher-order scattering is the diffraction from the surface

discontinuity between the parabolic region of the reflector and the rolled edge. This discontinuity is quite subtle in that cosine-squared blending ensures that the radius of curvature, as well as its first three derivatives, are all continuous at the junction point. Therefore the diffraction due to the junction is quite small, and the endpoint contributions must be primarily responsible for the offset and oscillations seen in the total PO field.

Fig. 26b shows the total PO field after the first-order endpoint contribution is removed. Note that the amplitude of the oscillations is greatly diminished. The results of first-order correction followed by second-order correction is shown in Fig. 26c. The second-order correction was done using "a" as obtained by the technique of Section 3. Here the oscillations have diminished in both strength and number, and no offset can be observed. Thus, the significant endpoint contributions have now been removed, and the fields remaining are a close approximation to the legitimate higher-order scattered fields.

Also shown in Fig. 26c is the result when first- and second-order endpoint correction is done, but "a" is assumed to be constant. Here, "a" was chosen to be equal to the actual value in the principal plane on the top side of the reflector. In this case the approximation is quite good. This is to be expected since the variation in "a" along the shadow boundary contour of the main reflector is small.

Fig. 26d shows the higher-order scattered fields in the principal plane, as well as the GO field. This pattern was obtained by subtracting the GO field from the total PO field after first- and second-order endpoint correction. Well into the target zone, these fields are approximately 40 dB below the magnitude of the GO field. Thus, this compact range would be suitable for determining the radar cross section of low-observables. This determination would be hard to make if accurate endpoint correction were not available.

Also shown in Fig. 26d are the higher-order scattered fields calculated using the constant-"a" approximation discussed above. Note that the fields determined this way are underestimated near the top, where the approximation is nearly exact. Conversely, the fields are

overestimated near the bottom, where the approximation is less appropriate. It is unwise to draw any conclusions based on the patterns near the center of the cut, since the magnitude of the fields in this region are of the order of the numerical error generated in the calculation.

- **Vertical Cut at $x = -2.5ft$**

  The fields obtained in this case are shown in figures 27a through 27d. In this cut, the same observations are made as in the previous case. An interesting difference exists between this cut and the principal plane cut, however. Note in Fig. 27c that the higher-order scattering is slightly stronger in this cut. This is due to the proximity of this cut to the junction contour.

  In this cut, the "constant-a" approximation causes the higher-order scattering to be overestimated over much of the cut.

- **Horizontal Cut at $y = 6.5ft$**

  This cut is at the center height of the main reflector. The fields obtained are shown in figures 28a through 28d. Since this system is symmetric about the principal plane, field patterns for horizontal cuts are symmetric about $x = 0$.

  In this cut, the constant-a approximation causes the higher-order scattering to be over-estimated.

- **Horizontal Cut at $y = 8.294ft$**

  Finally, consider a horizontal cut near the top edge of the target zone. The fields in this cut are shown in figures 29a through 29d. In this case, the first- and second-order endpoint correction have the same effects as for the previous horizontal cut. Also note that this cut, like the vertical cut at $x = -2.5ft$, is relatively close to a junction contour, yielding slightly stronger higher-order scattering.

  Since the approximated value of "a" is close to the exact values of "a" for endpoints near this cut, the results using the approximation are quite good.

Above it was shown that the results obtained using endpoint correction with continuously-varying radius of curvature are quite reasonable. In the case of this compact range system, it was noted that the scattered fields obtained using a constant radius of curvature approximation were quite close to the true scattered fields. This is due to the small variation in "a" along the shadow boundary of the main reflector of this system. It was shown in Section 4, however, that the variation in "a" is often relatively large. Thus, only proper continuously-varying determination of "a" will consistantly yield the closest approximation to the true scattered fields.

6 Conclusions

In this report a technique has been described by which the radius of curvature "a" can be found for compact range reflectors with radially-attached rolled edges. This technique allows "a" to be found for all points on the shadow boundary contour. In Section 4 this technique was applied to a variety of basic reflector systems. All of these systems were vertically symmetric. In general, it was shown that "a" increases with distance from the main axis (i.e. the z-axis). Applying the technique to an offset-fed reflector with a circular junction contour, it was found that "a" is smoothly-varying with extrema occurring in the principal plane. Offset-fed reflectors with square and concave junction contours have "a"-variations which are similar to each other, and different from circular case. For these reflectors, the variation in "a" on the horizontal sides is greater than the variation on the vertical sides. Also, "a" can be discontinuous at corners, with the discontinuity becoming more serious with increasing offset. Finally, one may conclude that for offset-fed systems in general, "a" varies about the principal plane values from the center-fed case, and typically increases with increasing offset.

Having "a" available for the entire shadow boundary contour makes it possible to accurately calculate second-order endpoint contributions. In Section 5, the effects of these contributions on the total PO field in the target zone of a vertically-symmetric offset-fed compact range were seen. Four cuts with different locations and orientations were considered. In each case, it was found that first- and second-order endpoint correction

using the technique presented here for finding "a" leads to cancellation of the significant endpoint effects and therefore gives a better approximation to the true scattered fields. Furthermore, finding "a" at each point along the shadow boundary, as opposed to assuming "a" to be constant, is often nessessary for accurate results. The technique presented in Section 3 is useful in this respect.

References

[1] I.J. Gupta and W.D. Burnside, "A Physical Optics Correction for Backscattering from Curved Surfaces", IEEE Trans. on Antennas and Prop., Vol. AP-35, No. 5, May 1987.

[2] I.J. Gupta, C.W.I. Pistorius and W.D. Burnside, "An Efficient Method to Compute Spurious Endpoint Contributions in PO Solutions", IEEE Trans. on Antennas and Prop., Vol. AP-35, No. 12, Dec. 1987.

[3] C.W.I. Pistorius, *New Main Reflector, Subreflector and Dual Chamber Concepts for Compact Range Applications*, Ph.D. Dissertation, The Ohio State University, 1986.

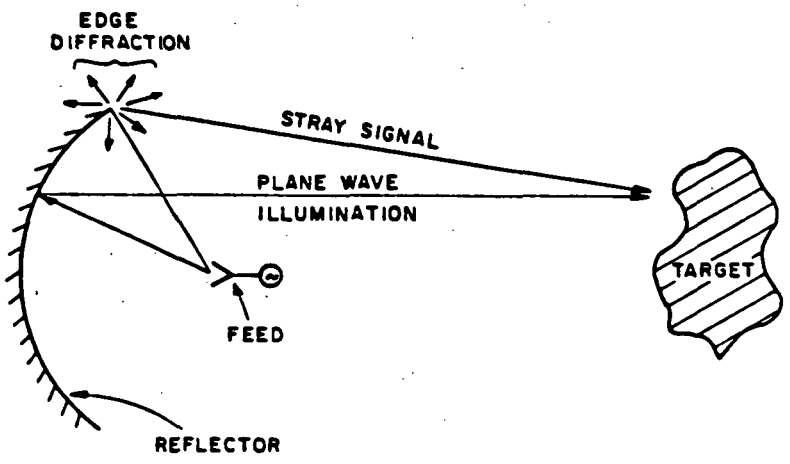

(a) Stray signal due to edge diffraction.

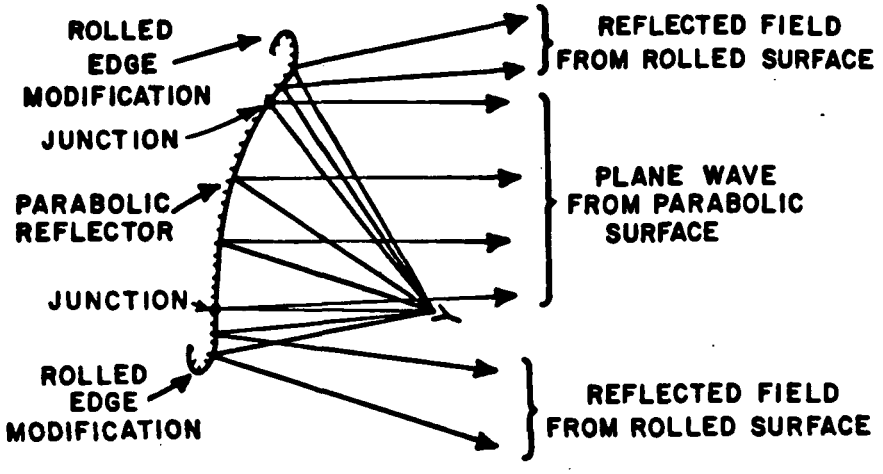

(b) Continuity of reflected field using rolled edges.

Figure 1: The use of rolled edge terminations to reduce diffraction into the target zone.

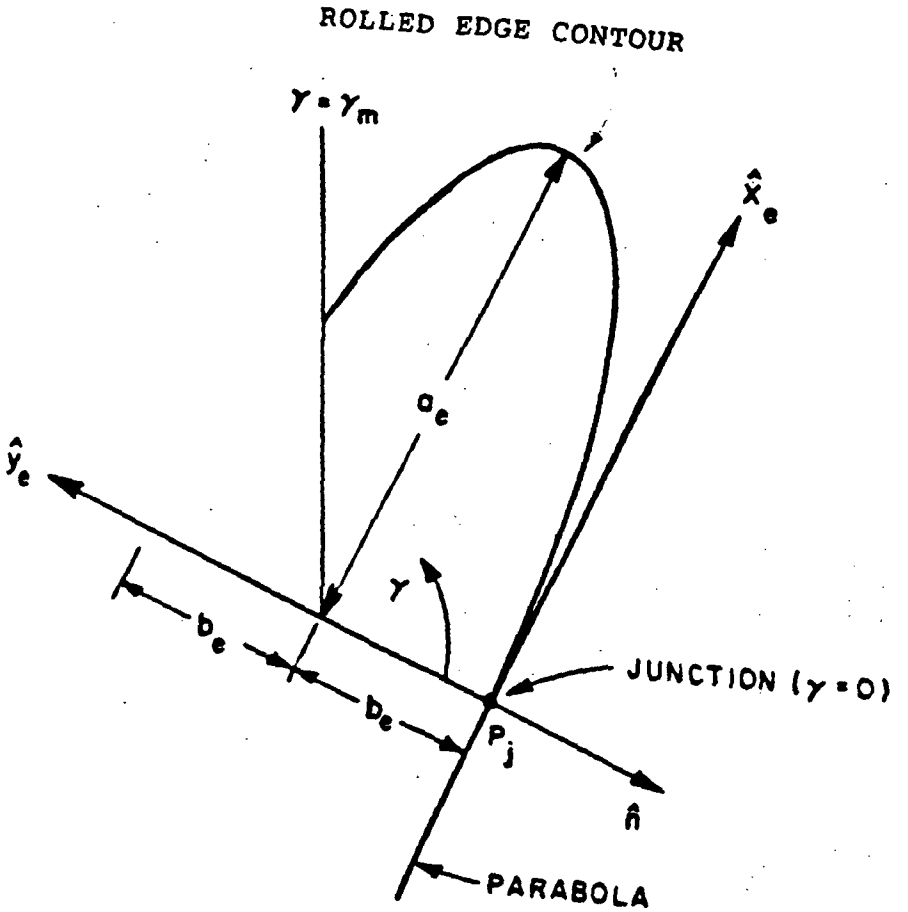

Figure 2: Rolled edge geometry.

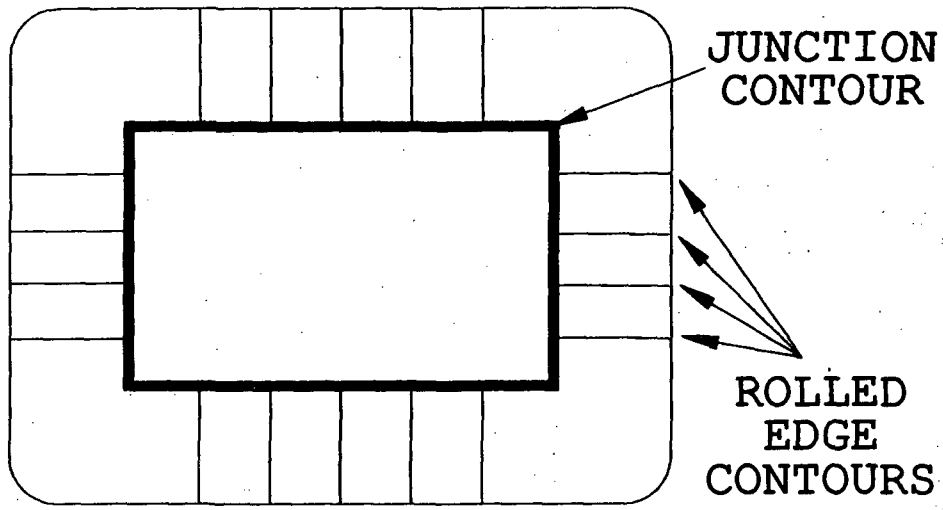

(a) Perpendicular attachment.

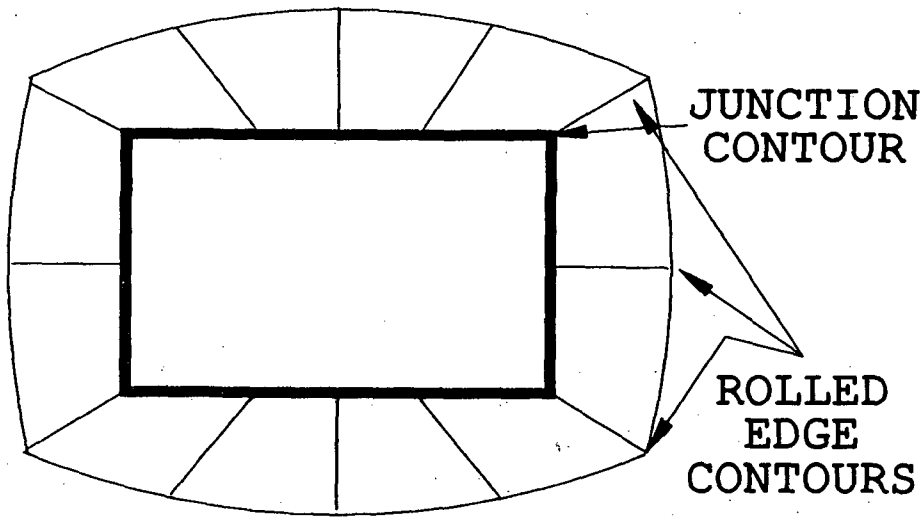

(b) Radial attachment.

Figure 3: Methods for adding rolled edge terminations.

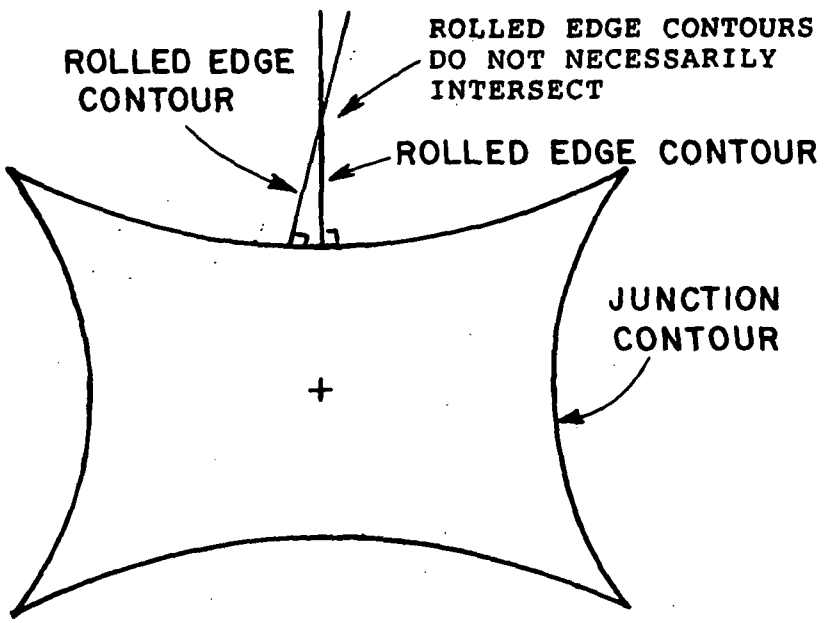

Figure 4: An example of multiple definition of the rolled edge surface when perpendicular attachment is used with concave rim-shapes.

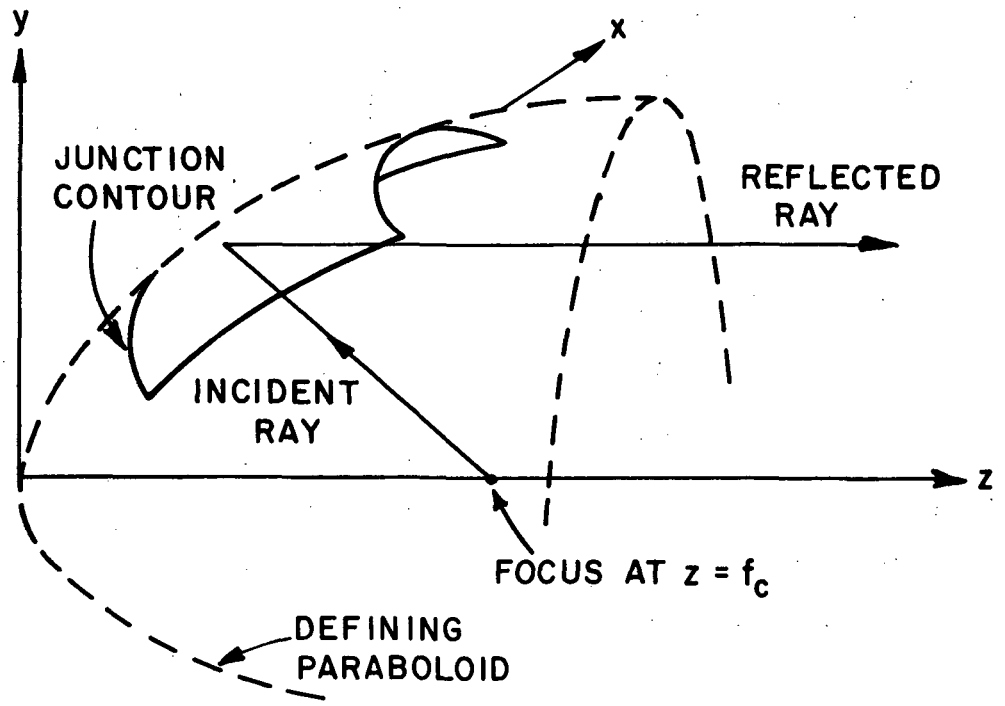

Figure 5: Geometry of the parabolic region.

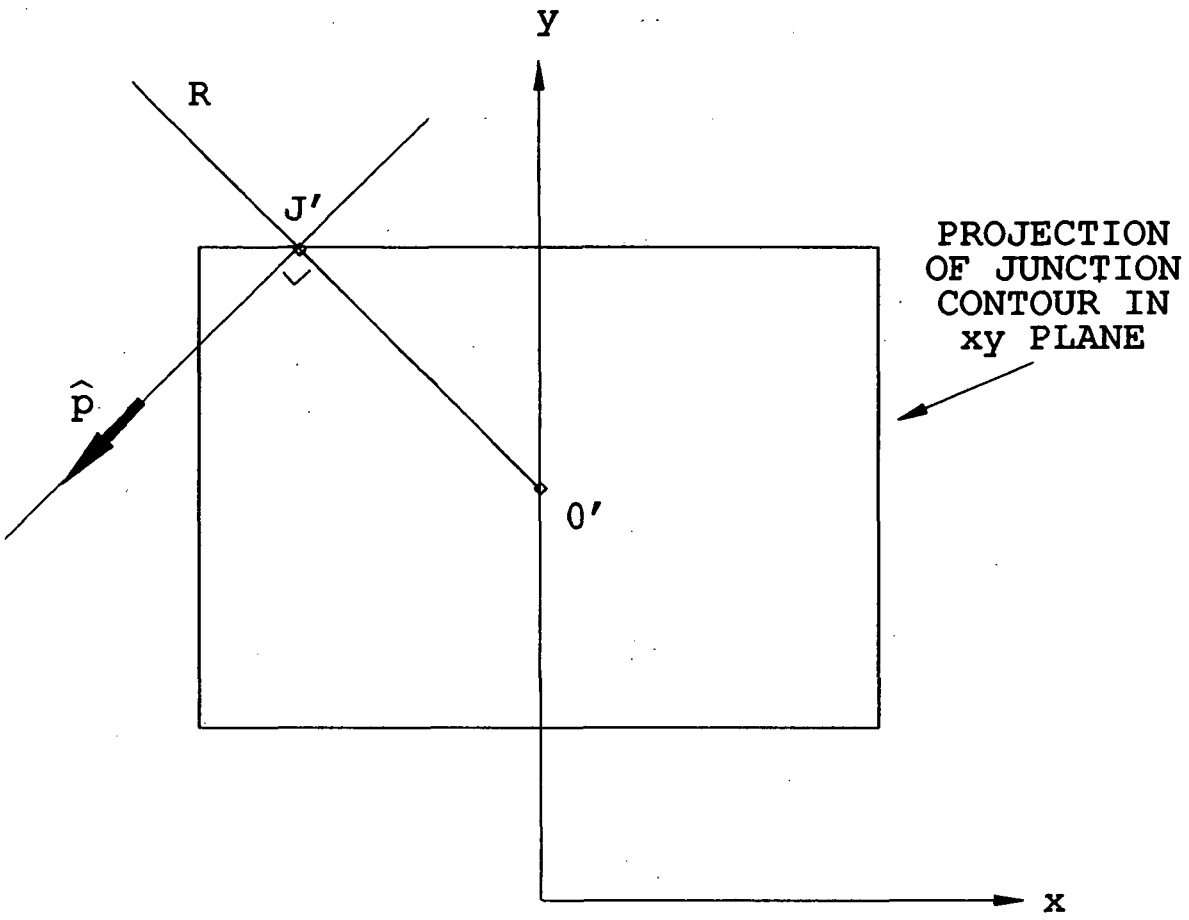

Figure 6: Defining $\hat{\mathbf{p}}$.

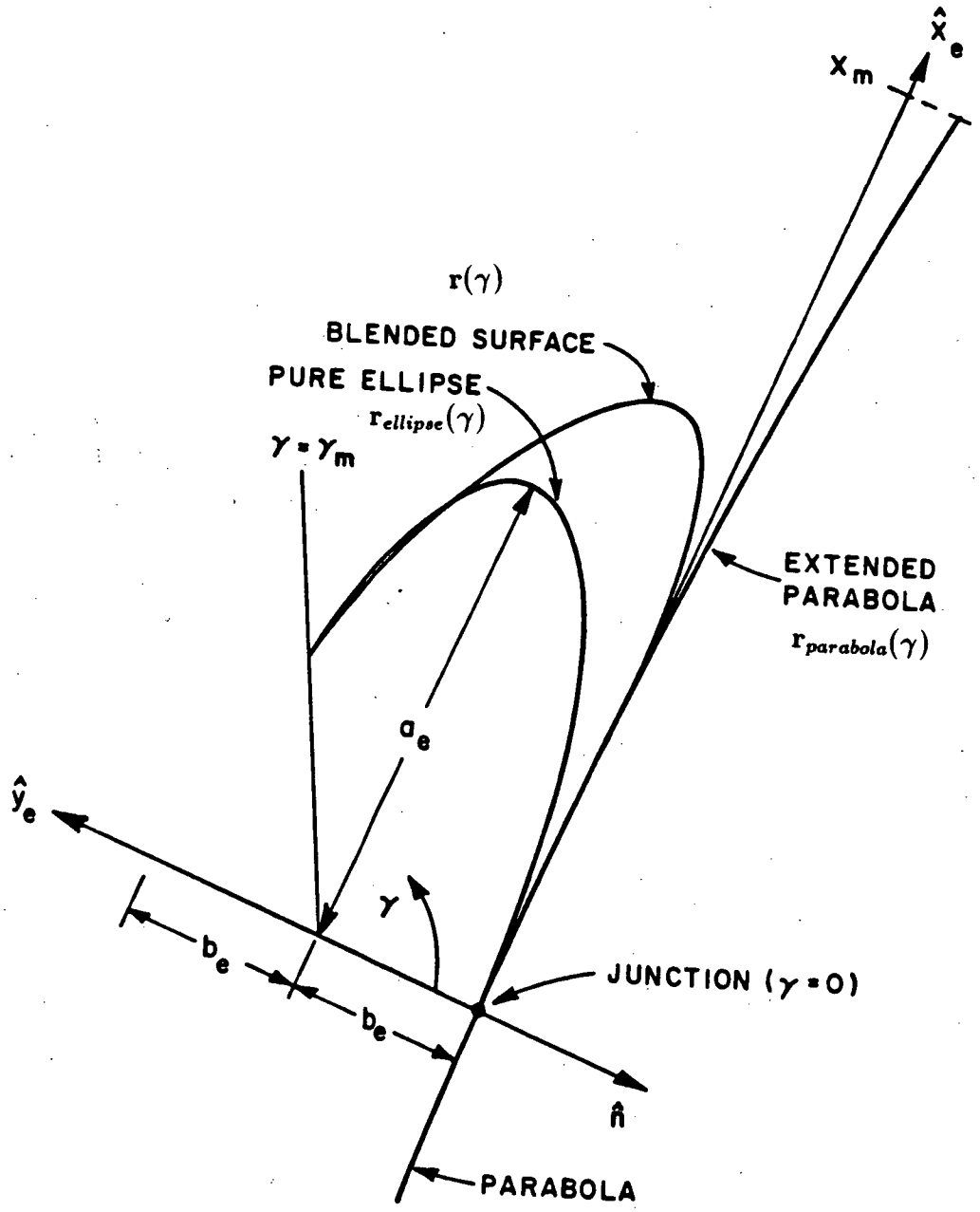

Figure 7: Blended rolled edge geometry.

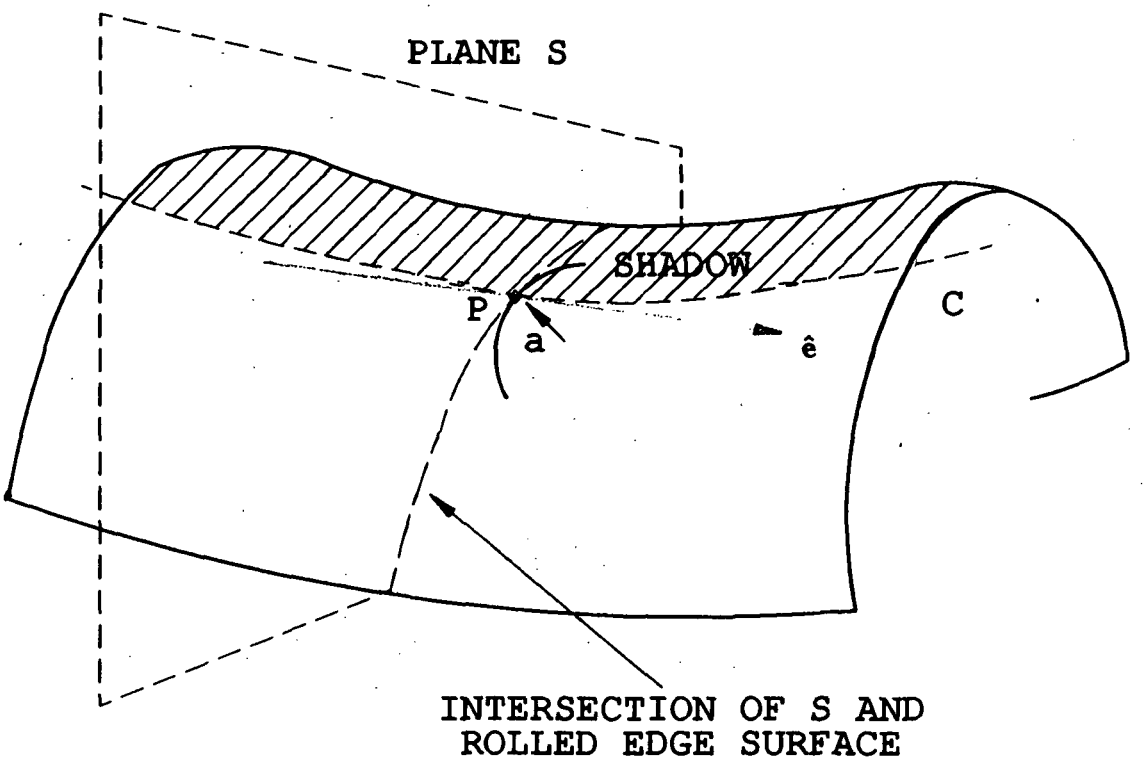

Figure 8: Defining the shadow boundary radius of curvature, "a".

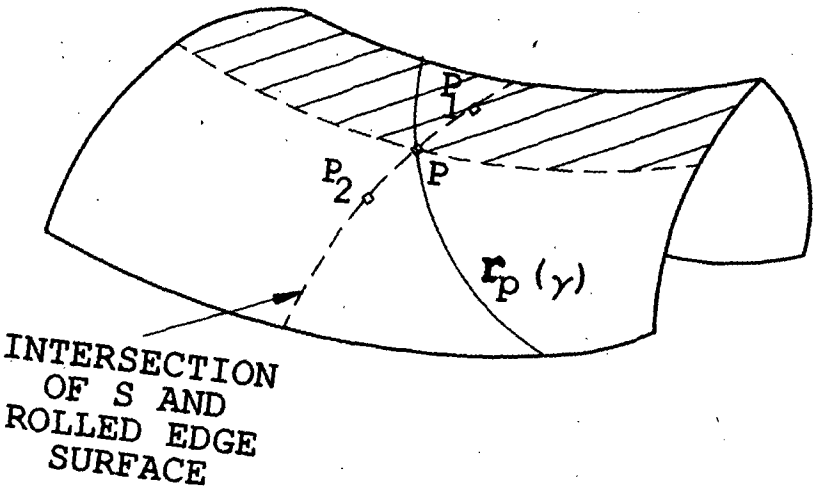

Figure 9: *A* case where $\mathbf{r}_P(\gamma)$ and S are not coincident.

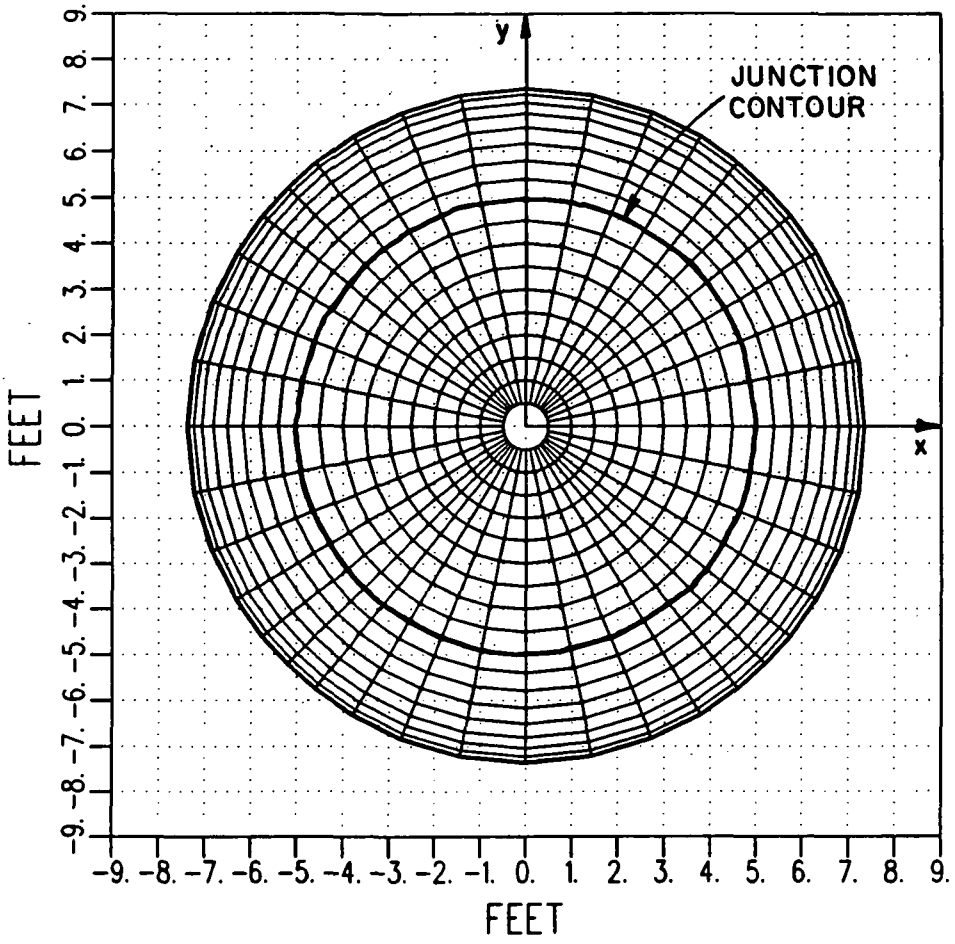

Figure 10: Center-fed main reflector with circular junction contour.

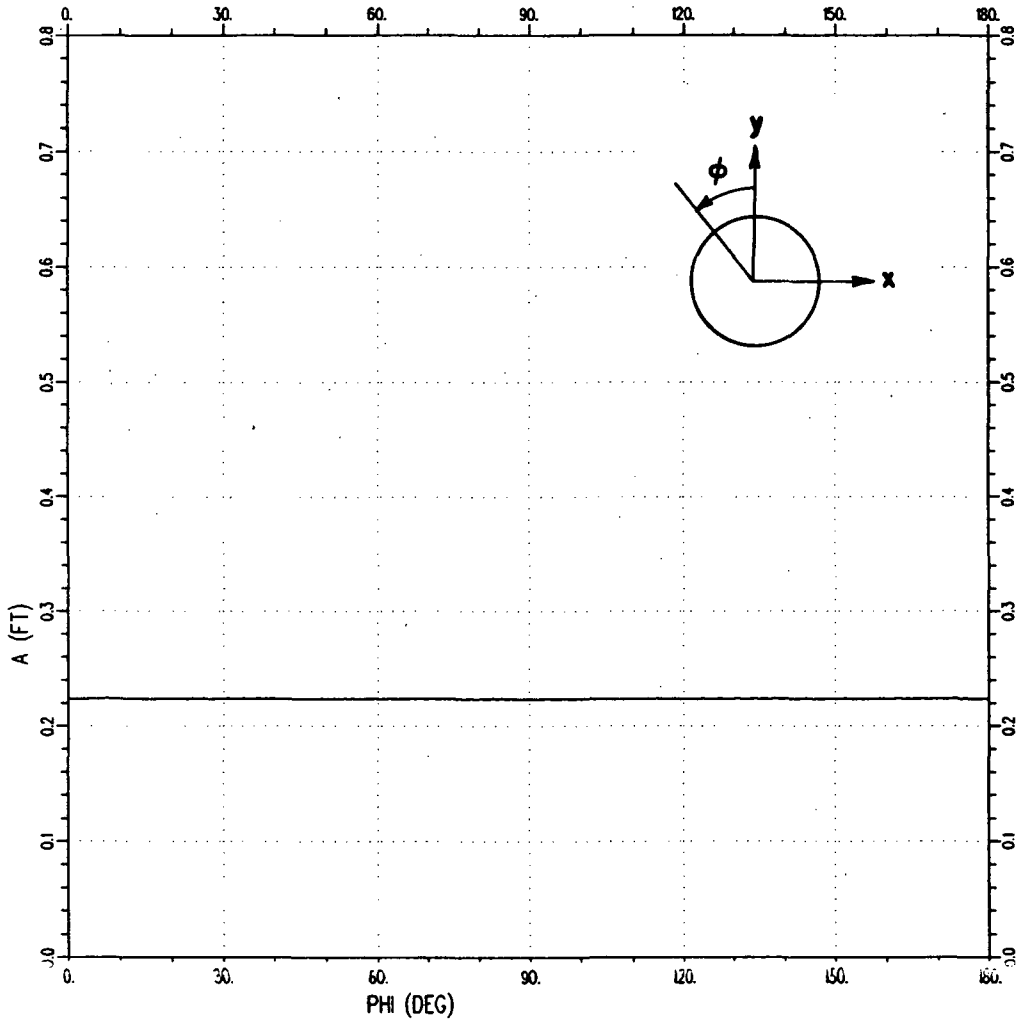

Figure 11: "a" along the shadow boundary contour of the center-fed main reflector with circular junction contour.

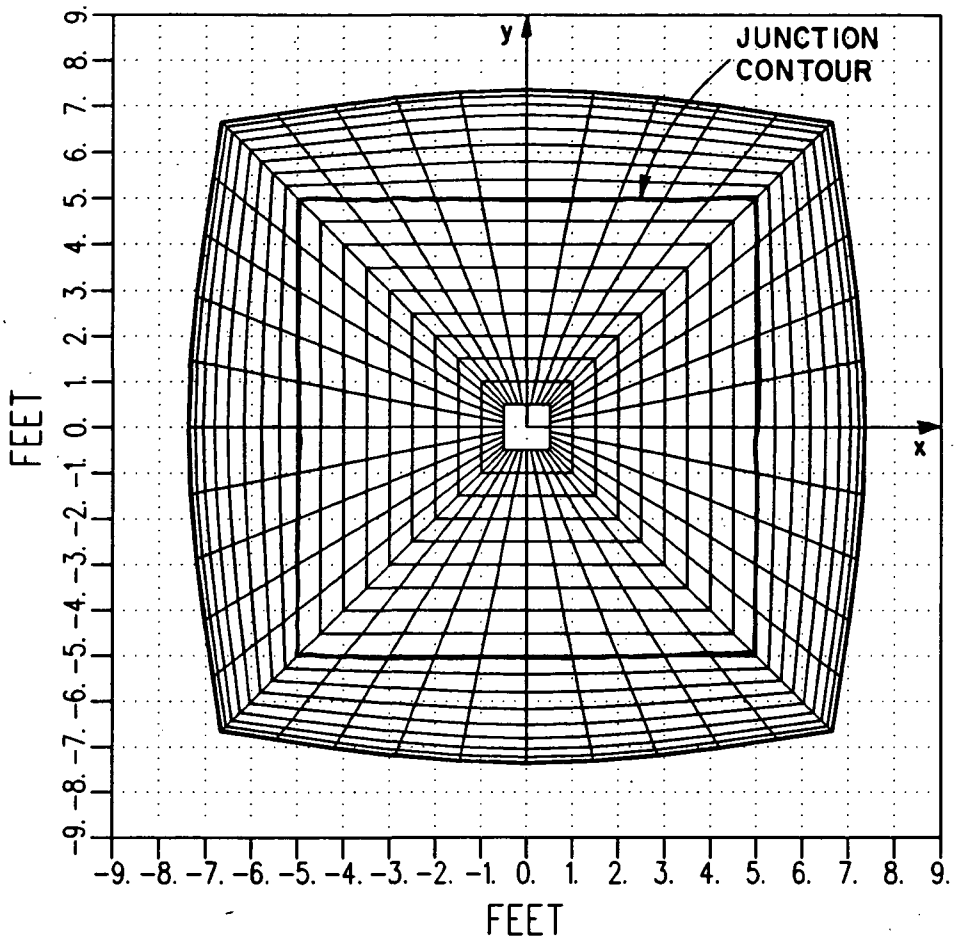

Figure 12: Center-fed main reflector with square junction contour.

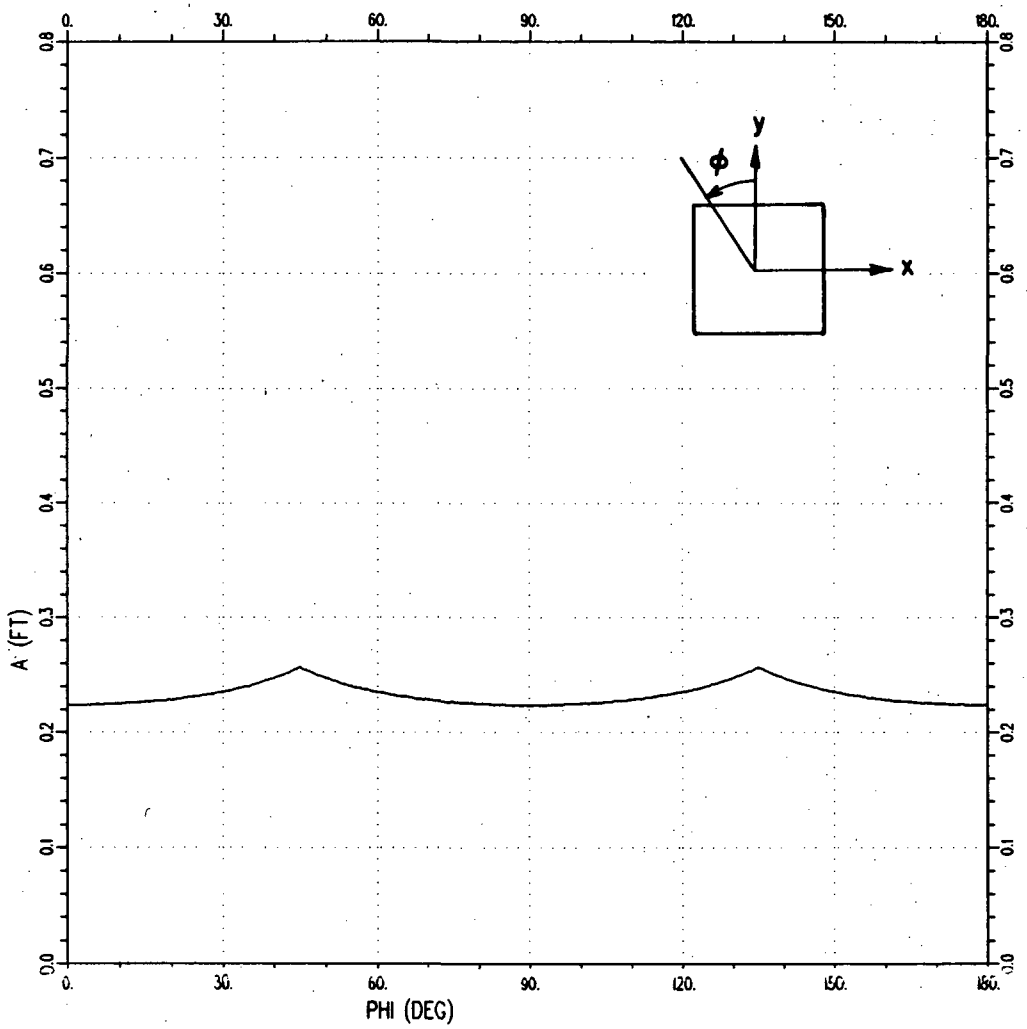

Figure 13: "a" along the shadow boundary contour of the center-fed main reflector with square junction contour.

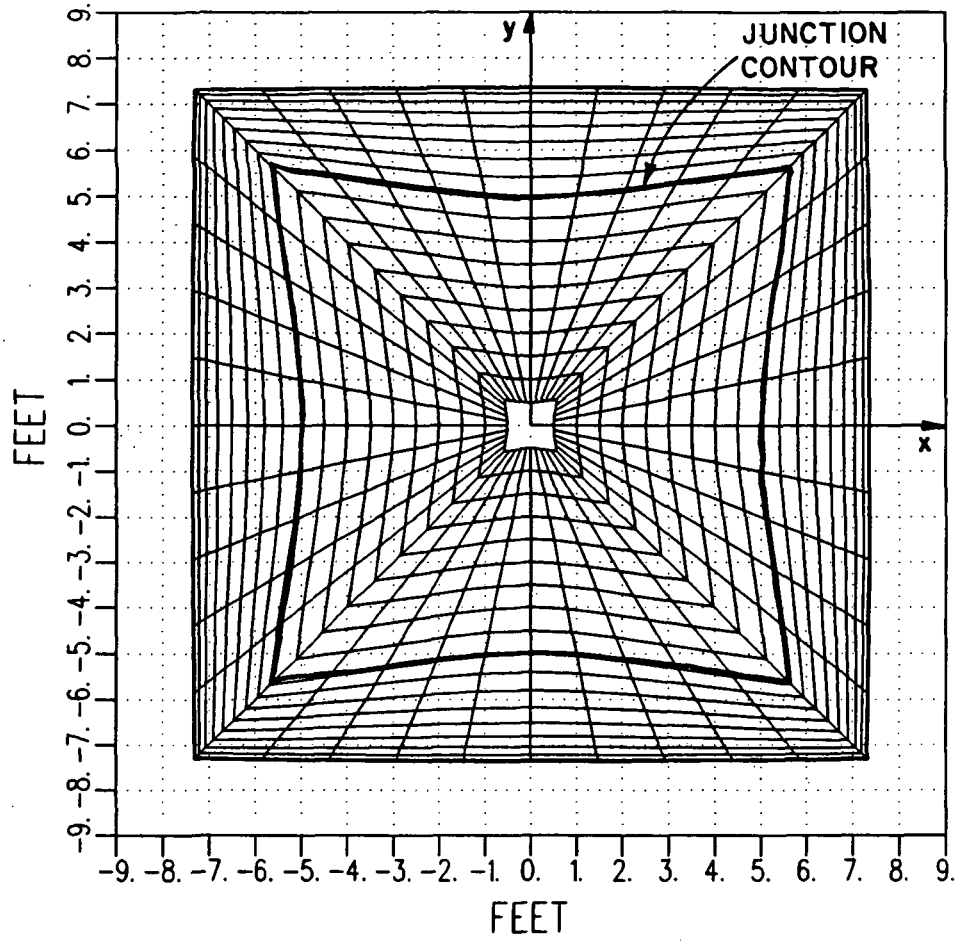

Figure 14: Center-fed main reflector with concave junction contour.

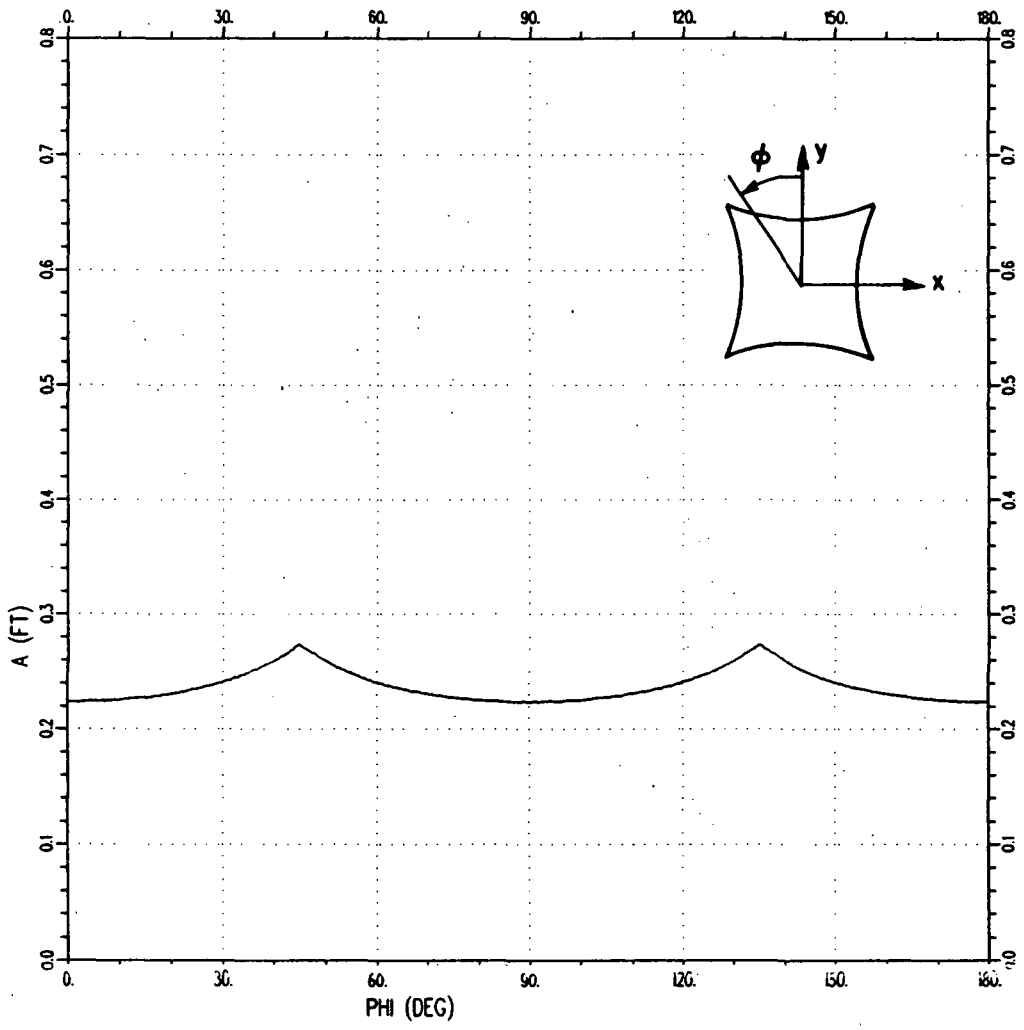

Figure 15: "a" along the shadow boundary contour of the center-fed main reflector with concave junction contour.

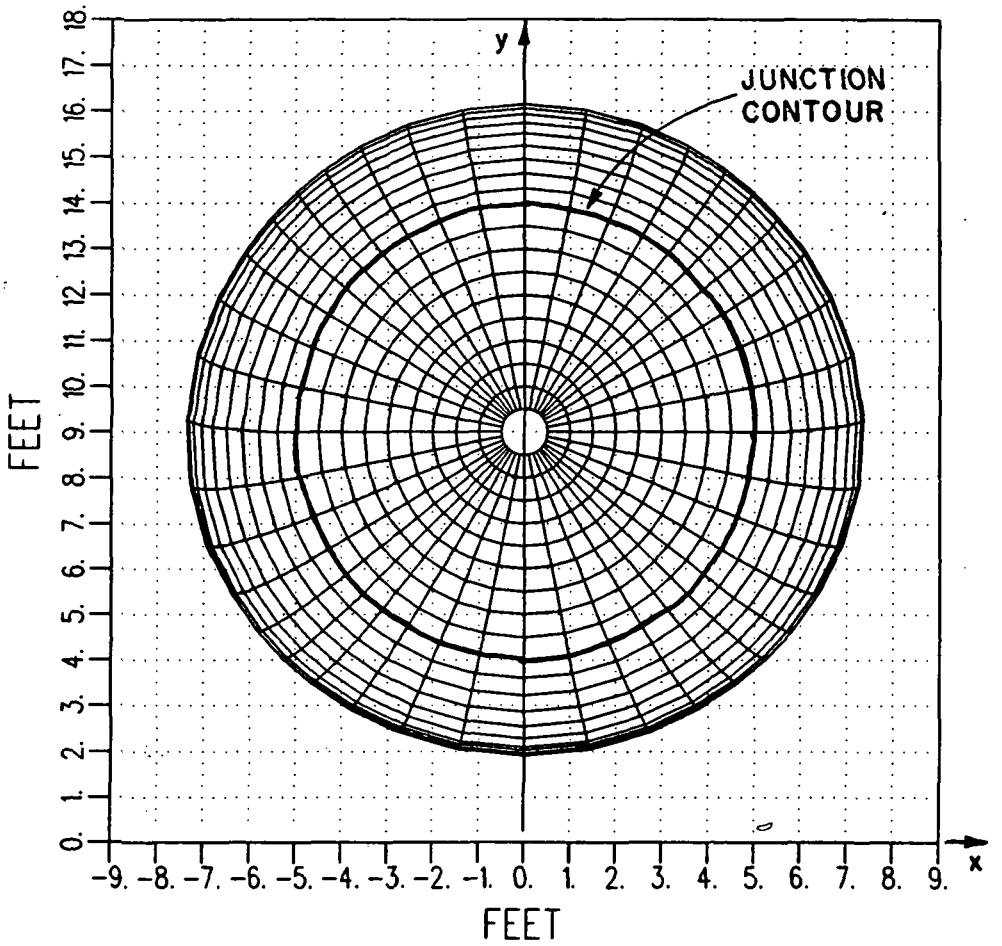

Figure 16: Main reflector with circular junction contour, vertically offset $9.0ft$.

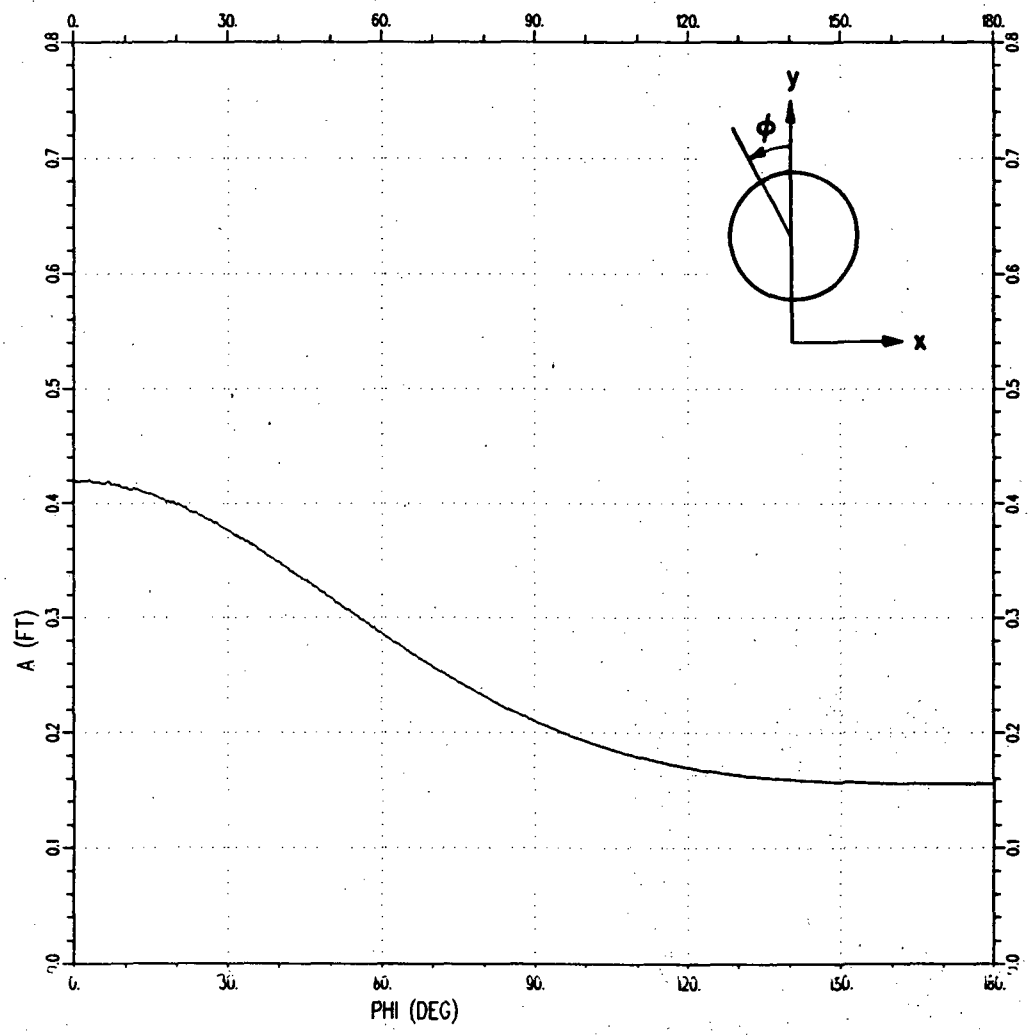

Figure 17: "a" along the shadow boundary contour of the offset-fed main reflector with circular junction contour.

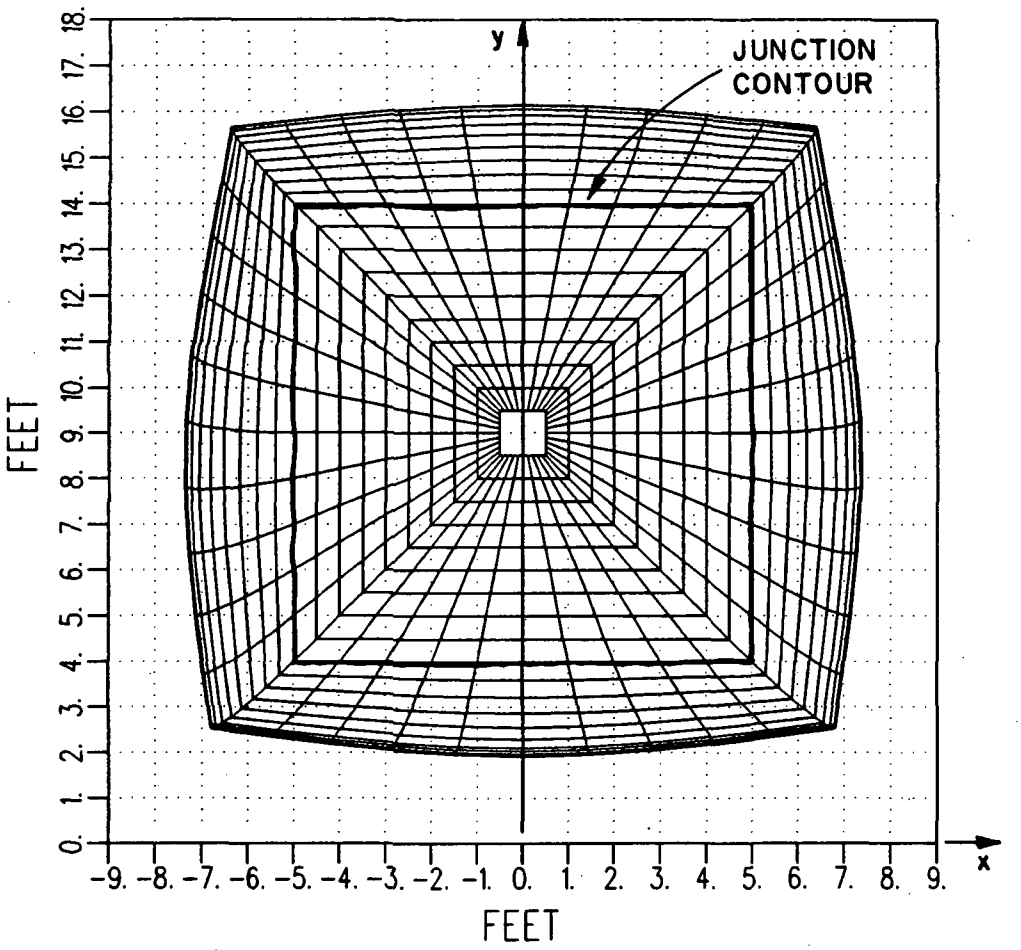

Figure 18: Main reflector with square junction contour, vertically offset $9.0ft$.

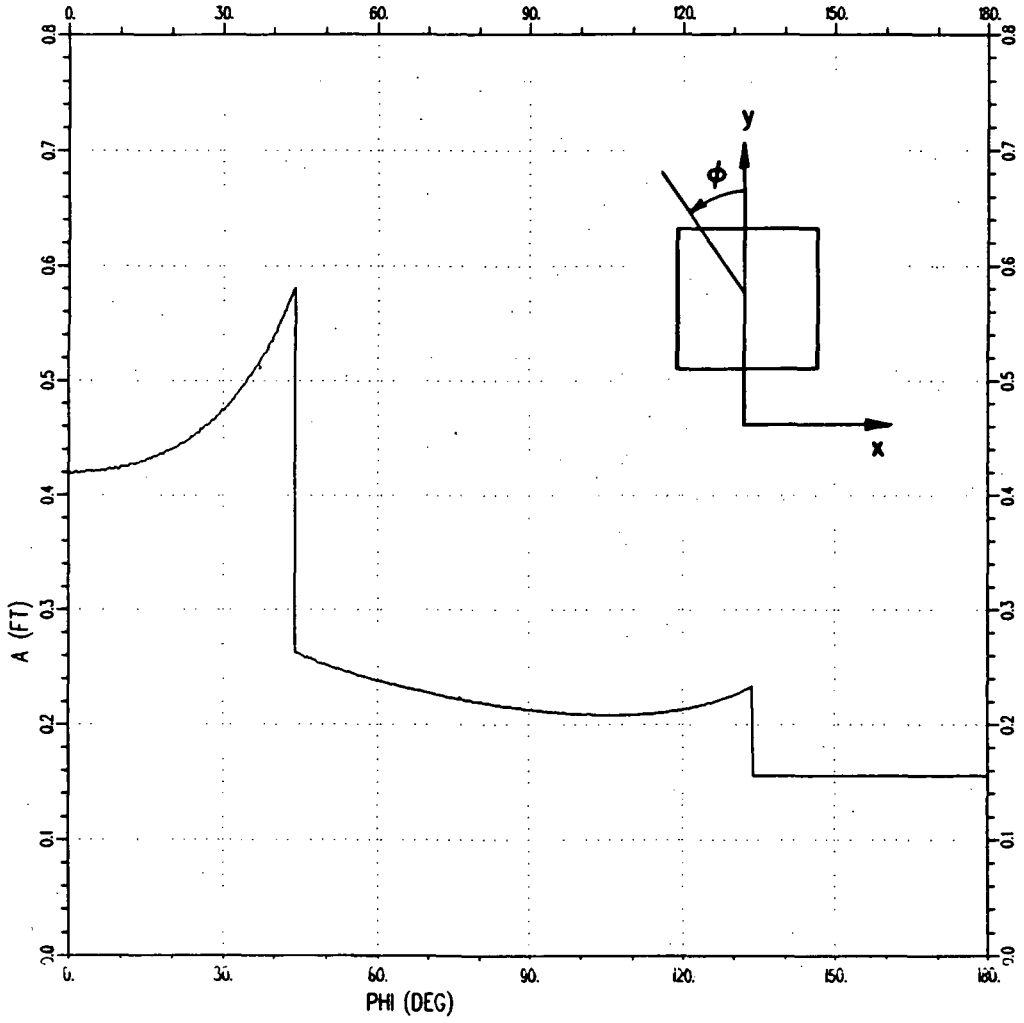

Figure 19: "a" along the shadow boundary contour of the offset-fed main reflector with square junction contour.

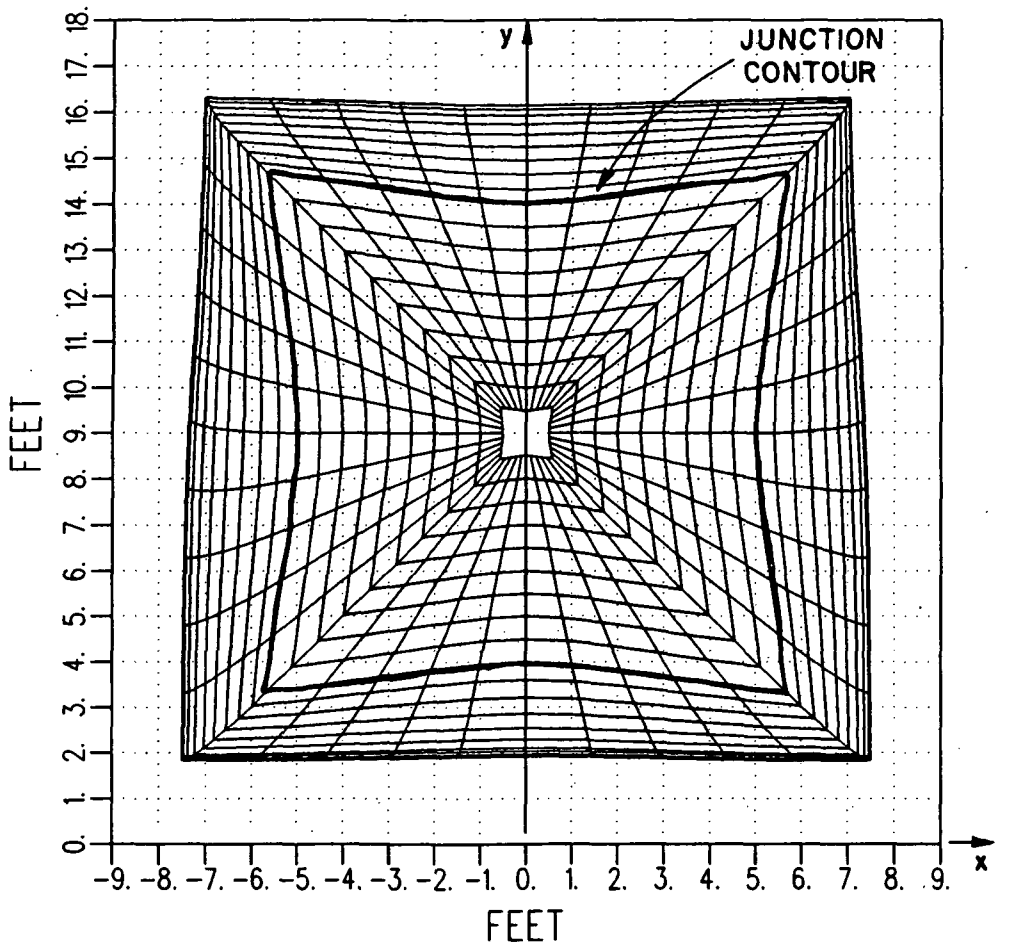

Figure 20: Main reflector with concave junction contour, vertically offset $9.0ft.$

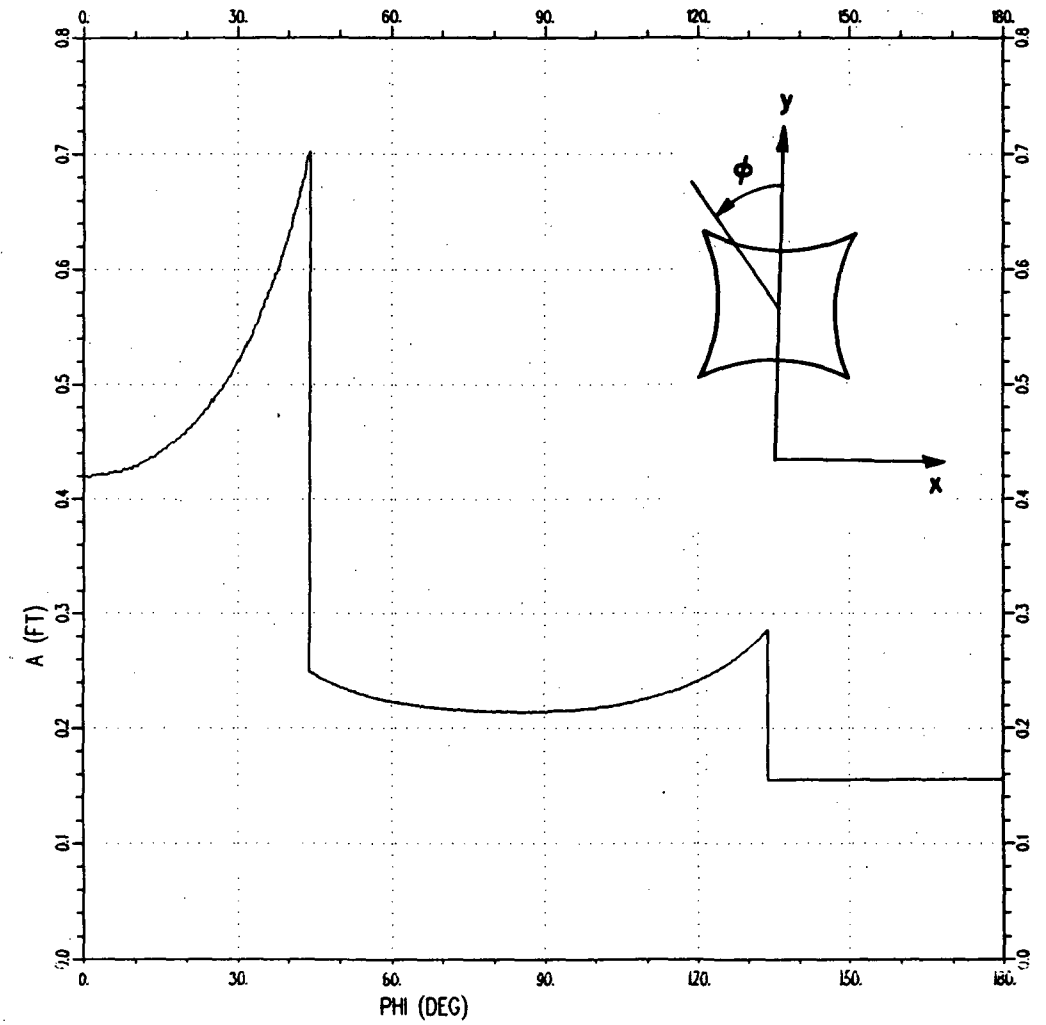

Figure 21: "a" along the shadow boundary contour of the offset-fed main reflector with concave junction contour.

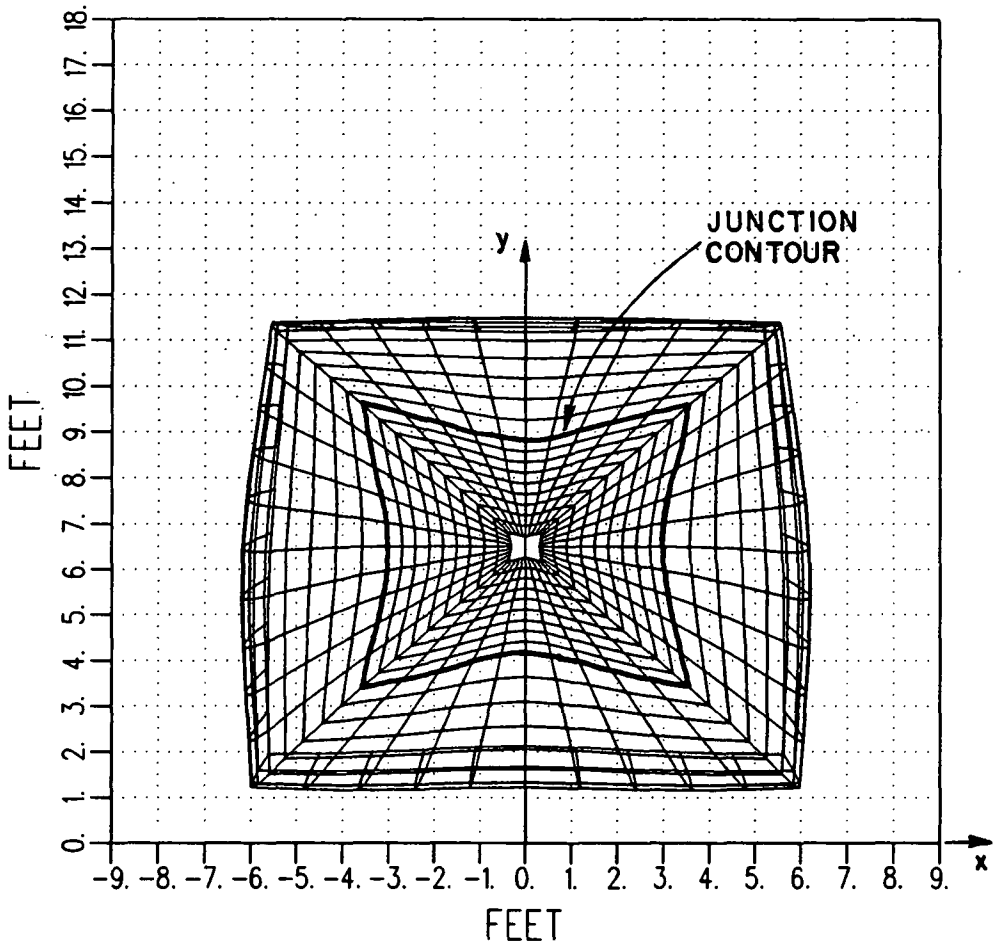

Figure 22: A small main reflector with concave junction contour, vertically offset $6.5ft$.

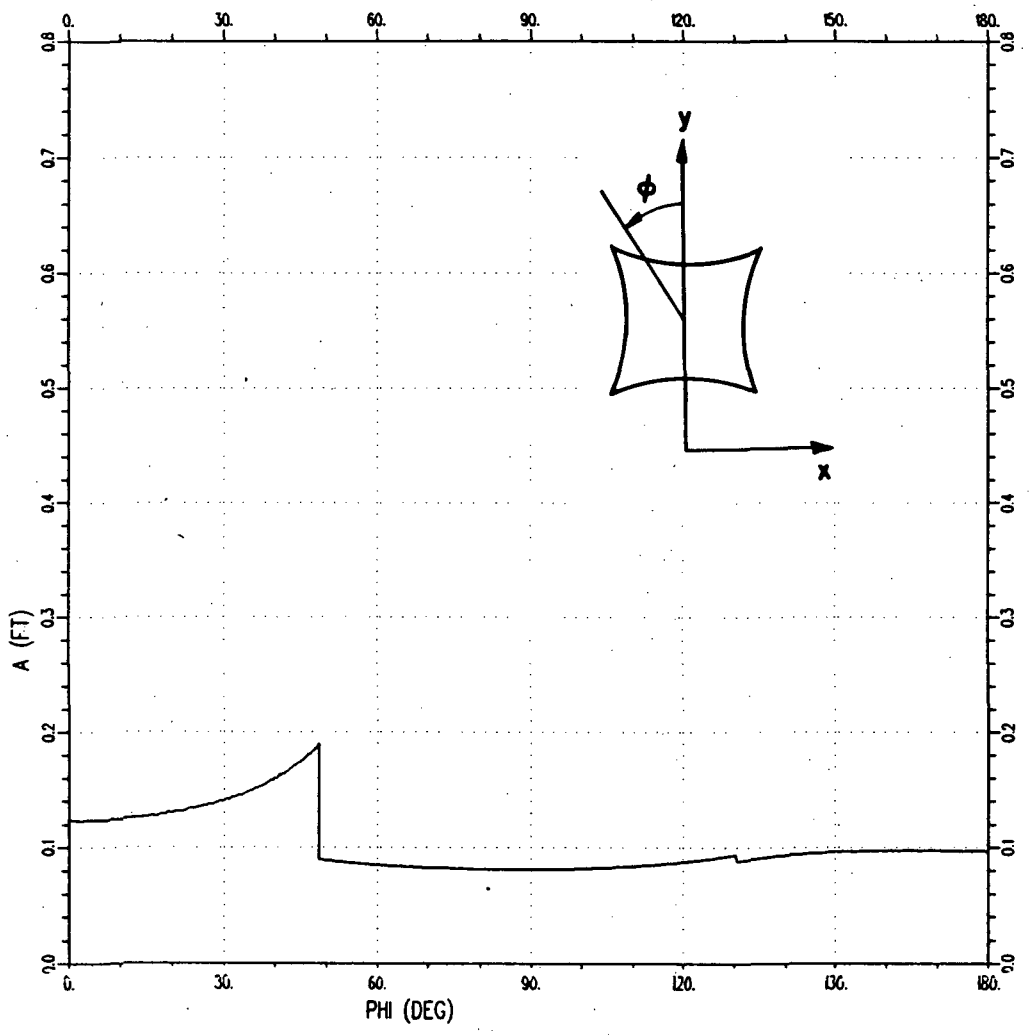

Figure 23: "a" along the shadow boundary contour of the small offset-fed main reflector with concave junction contour.

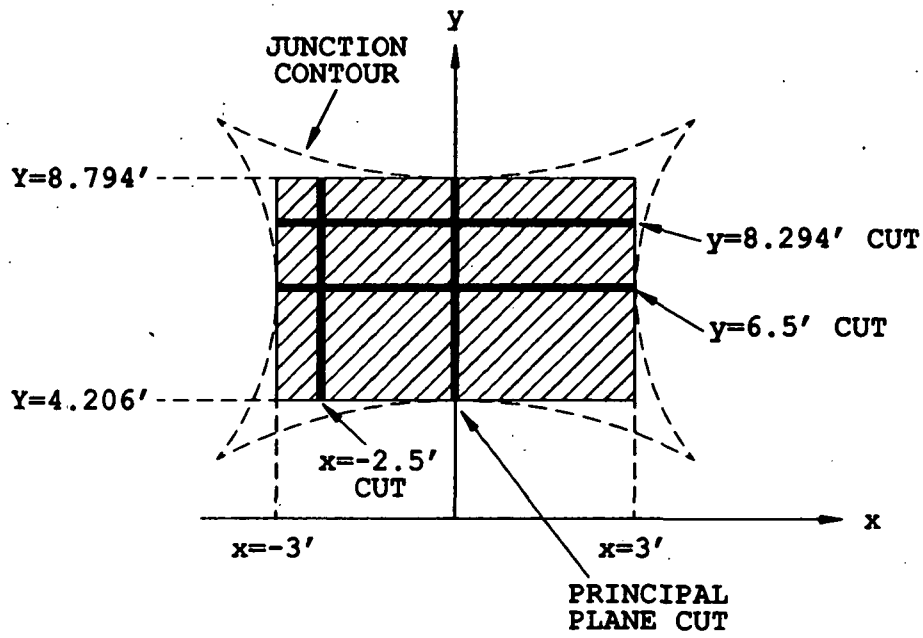

Figure 24: Cuts in which the scattered field has been computed. All cuts are in the $z = 15ft$ plane. The target zone is the shaded area.

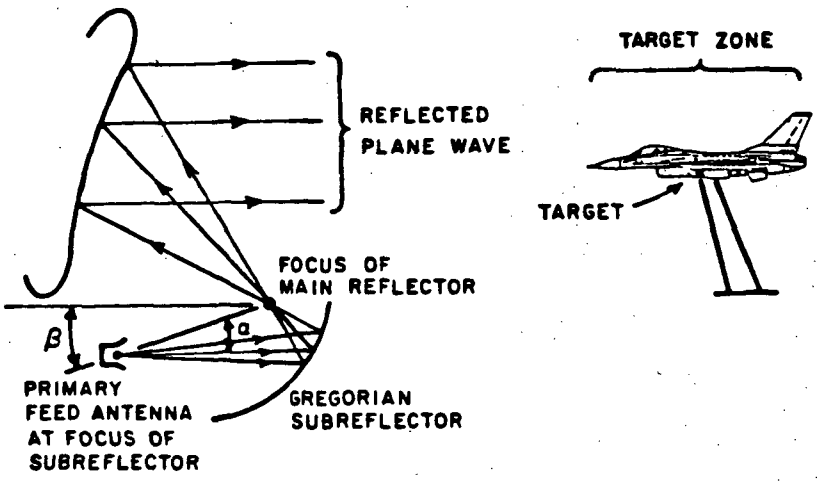

Figure 25: A compact range with a Gregorian subreflector feed system.

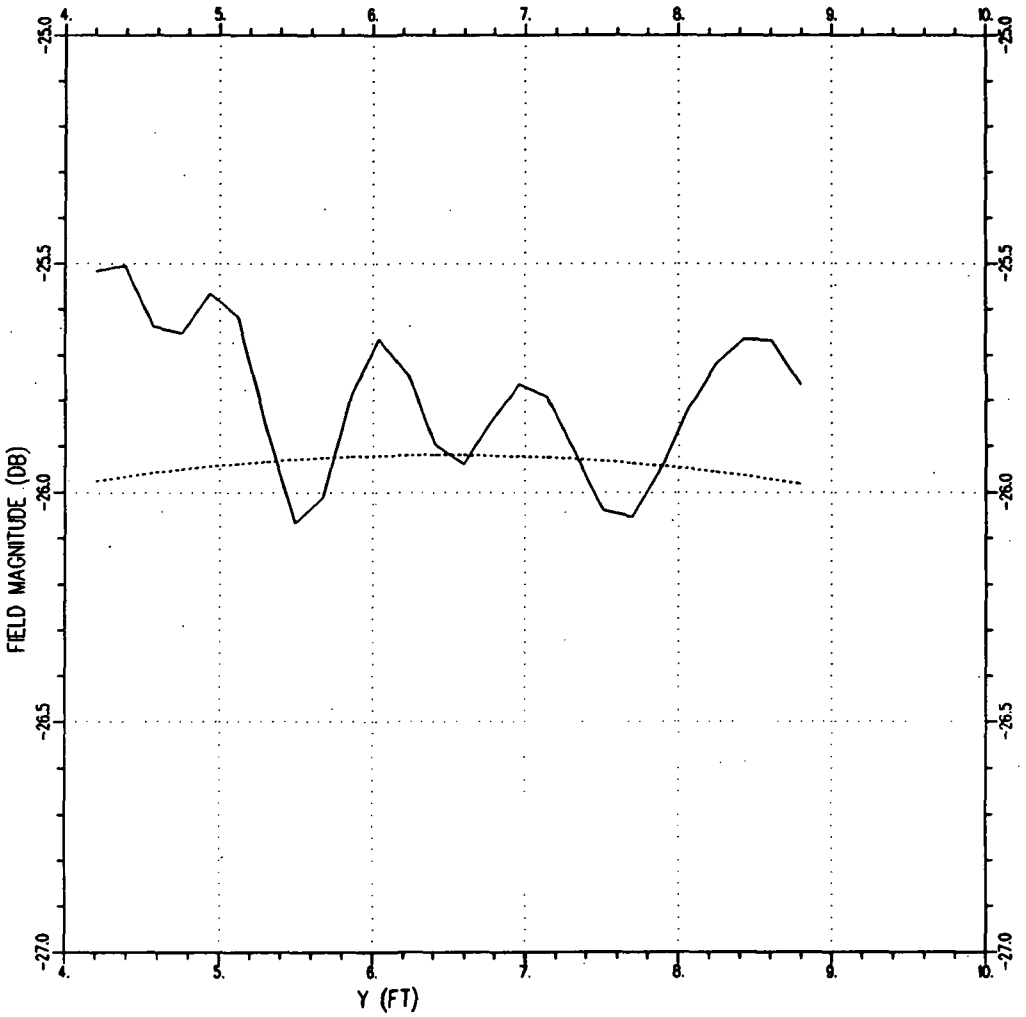

Figure 26(a): Total PO and GO fields along principal plane cut.

Total PO ——————

GO ·····

y-component shown.

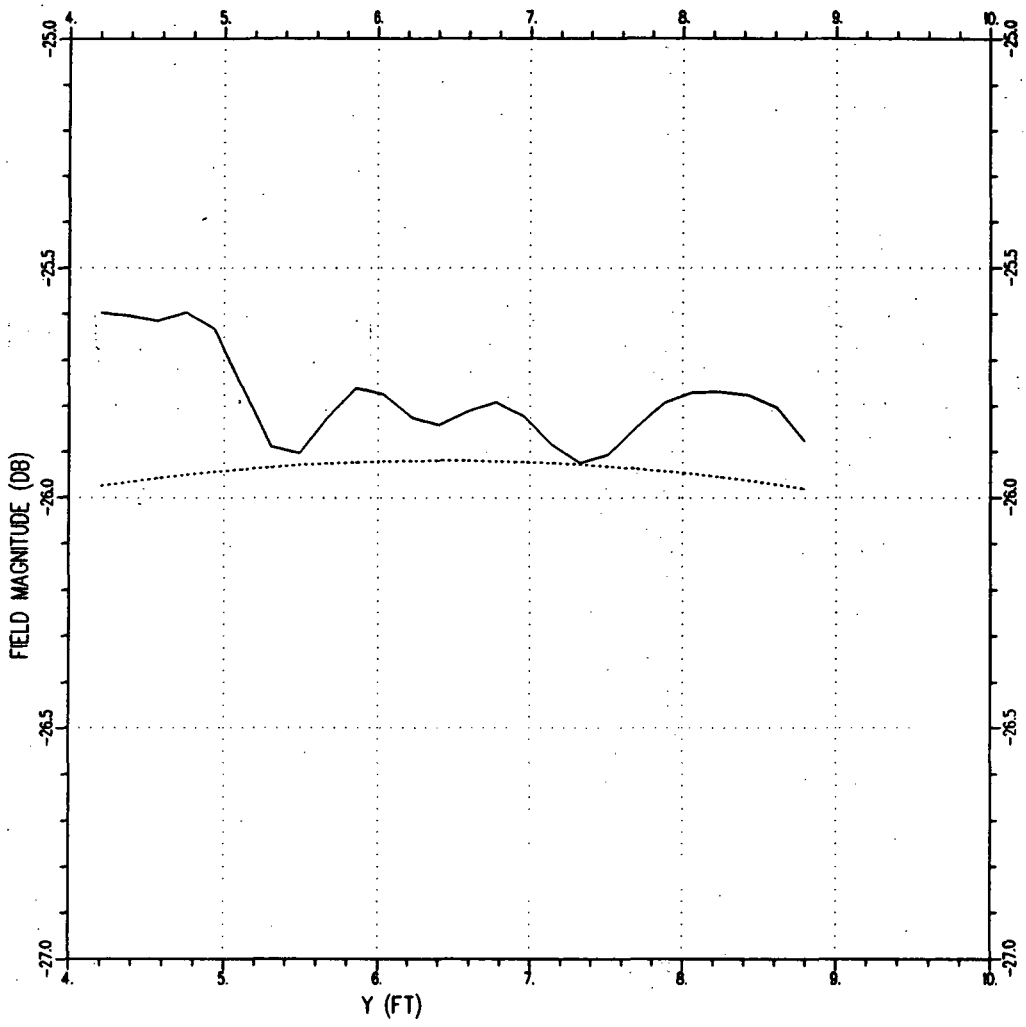

Figure 26(b): Total PO field along principal plane cut after first-order endpoint correction.

Total PO field after first-order endpoint correction ——————

GO ----------

y-component shown.

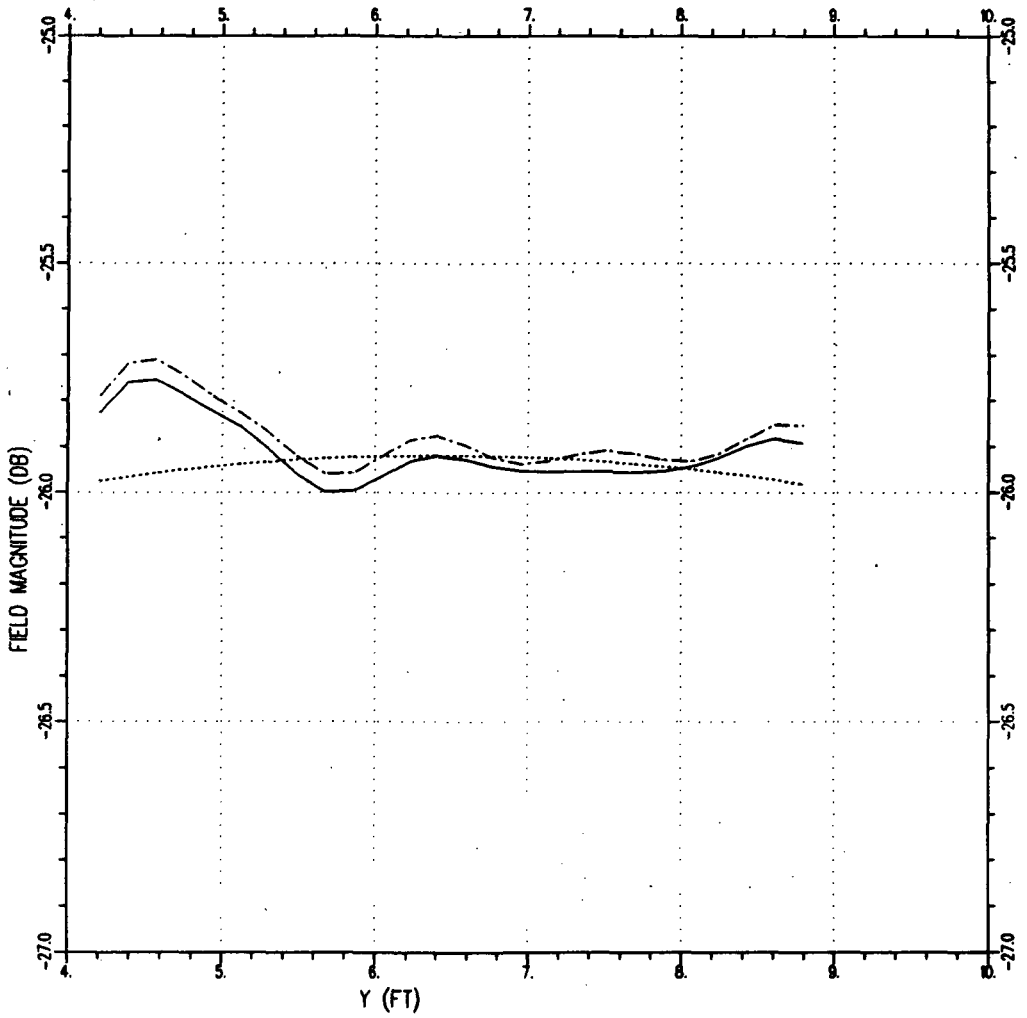

Figure 26(c): Total PO field along principal plane cut after first- and second-order endpoint correction.

Total PO after first- and second-order endpoint correction ————————

Total PO after first- and approximate second-order endpoint correction —·—·—·—·—

GO ·····

y-component shown.

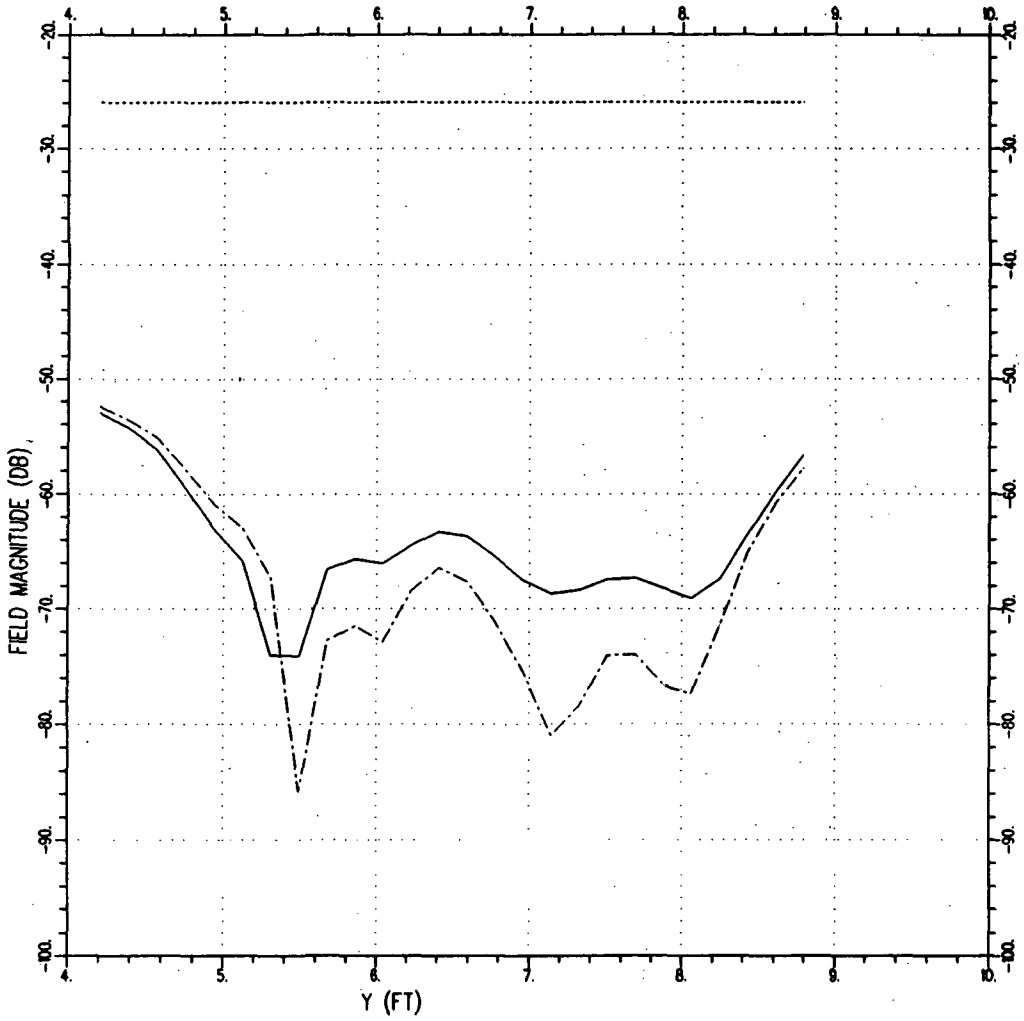

Figure 26(d): Higher-order scattered fields along principal plane cut.

Higher-order scattered fields ————————

Higher-order scattered fields using first- and approximate second-order endpoint correction —·—·—·—·—

GO .....

y-component shown.

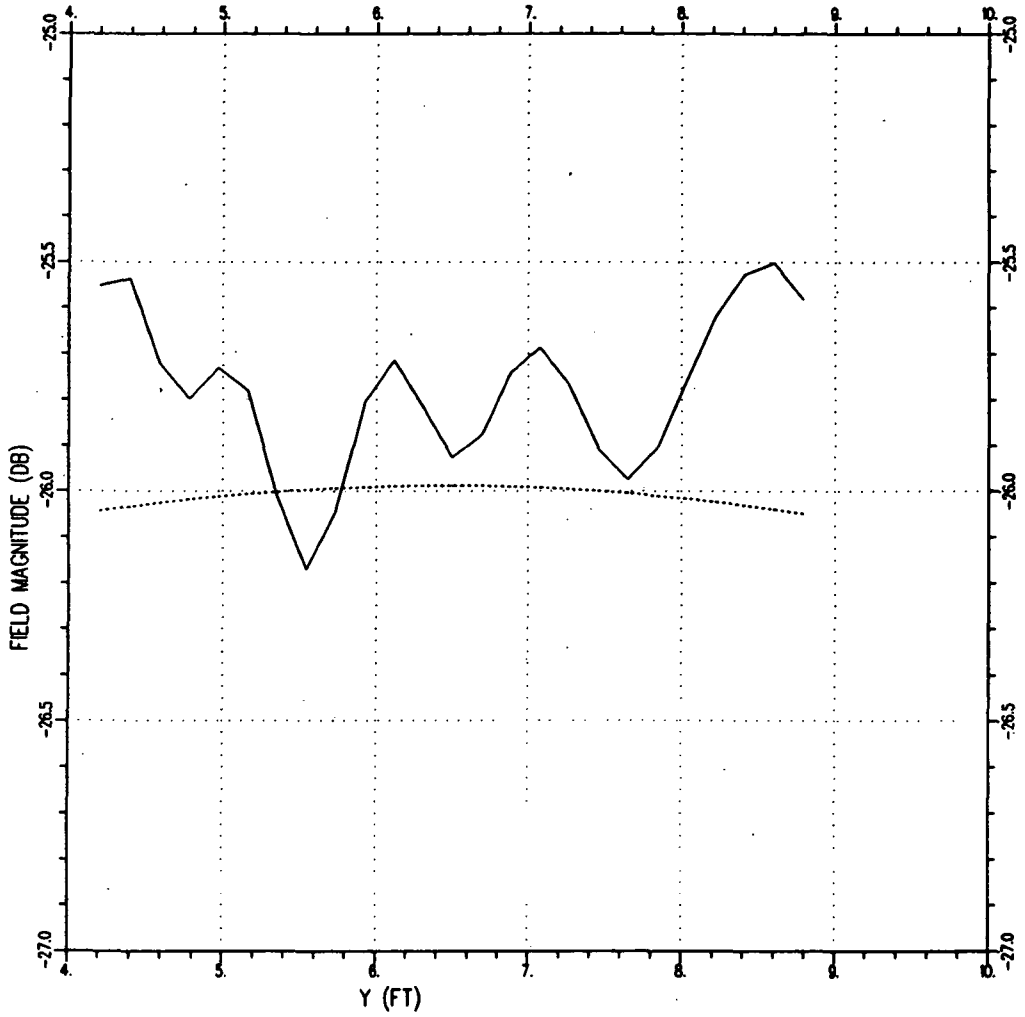

Figure 27(a): Total PO and GO fields along the $x = -2.5ft$ cut.

Total PO ————————

GO ····------····

y-component shown.

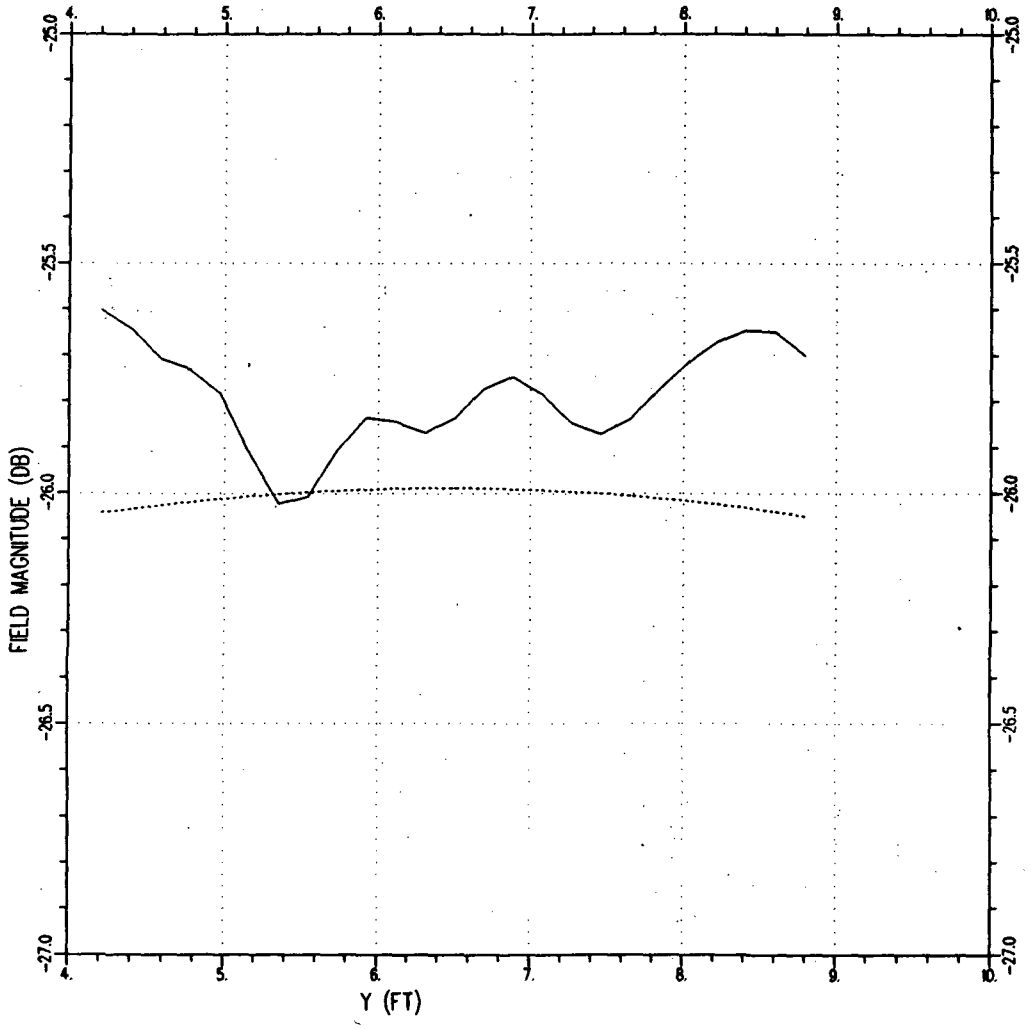

Figure 27(b): Total PO field along the $x = -2.5ft$ cut after first-order endpoint correction.

Total PO field after first-order endpoint correction. ————

GO ·····

y-component shown.

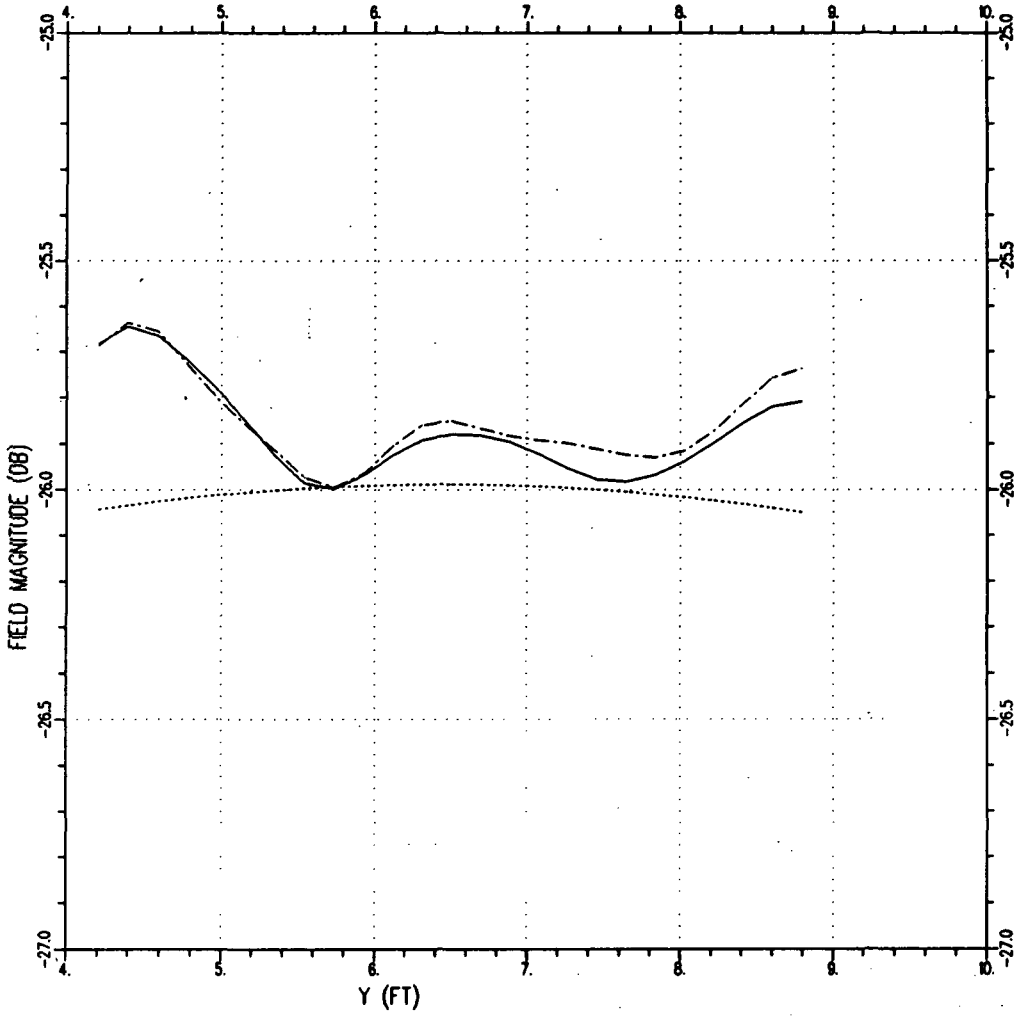

Figure 27(c): Total PO field along the $x = -2.5ft$ cut after first- and second-order endpoint correction.

Total PO after first- and second-order endpoint correction ————————

Total PO after first- and approximate second-order endpoint correction ..—.—.—.—.—.

GO .....

y-component shown.

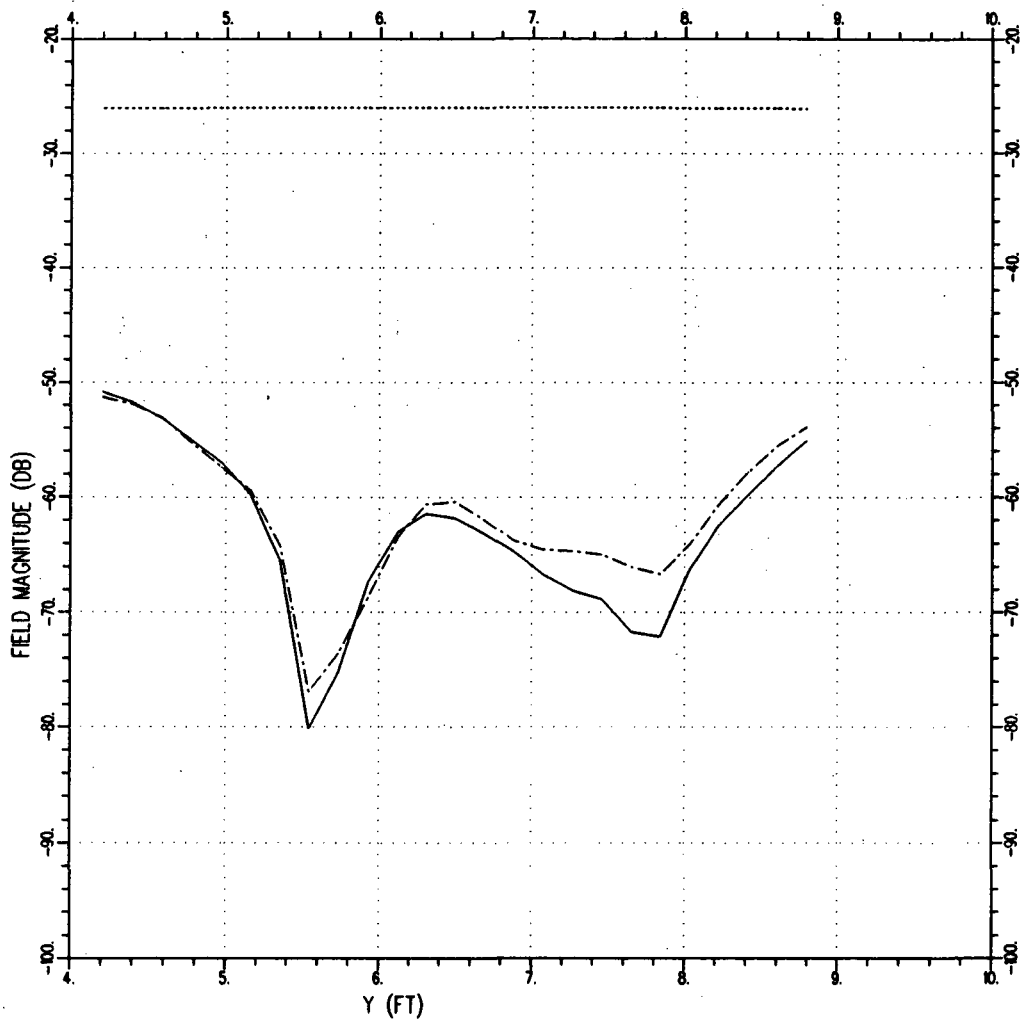

Figure 27(d): Higher-order scattered fields along the $x = -2.5ft$ cut.

Higher-order scattered fields ————————

Higher-order scattered fields using first- and approximate second-order endpoint correction —·—·—·—·—

GO .....

y-component shown.

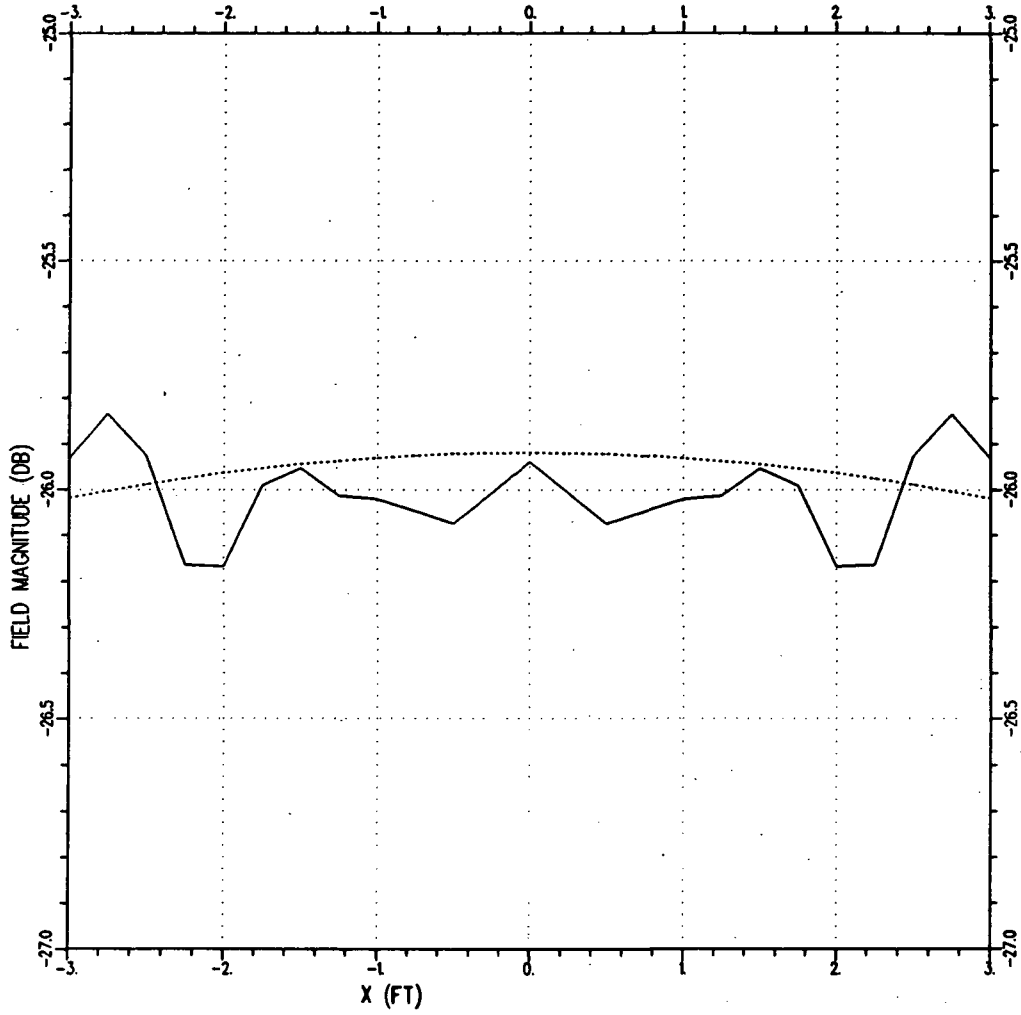

Figure 28(a): Total PO and GO fields along the $y = 6.5ft$ cut.
Total PO ————————
GO ····· ····· ·····
y-component shown.

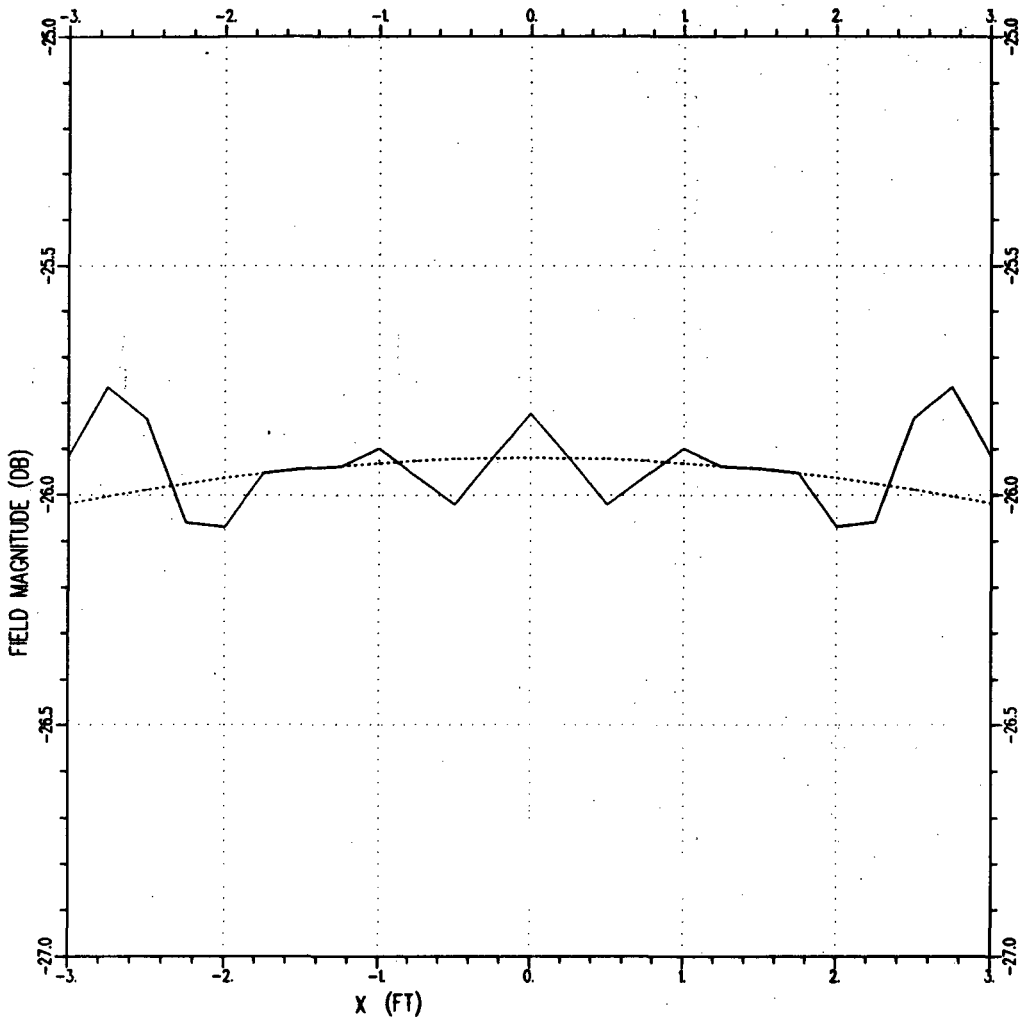

Figure 28(b): Total PO field along the $y = 6.5ft$ cut after first-order endpoint correction.

Total PO field after first-order endpoint correction. ————————

GO ·····

y-component shown.

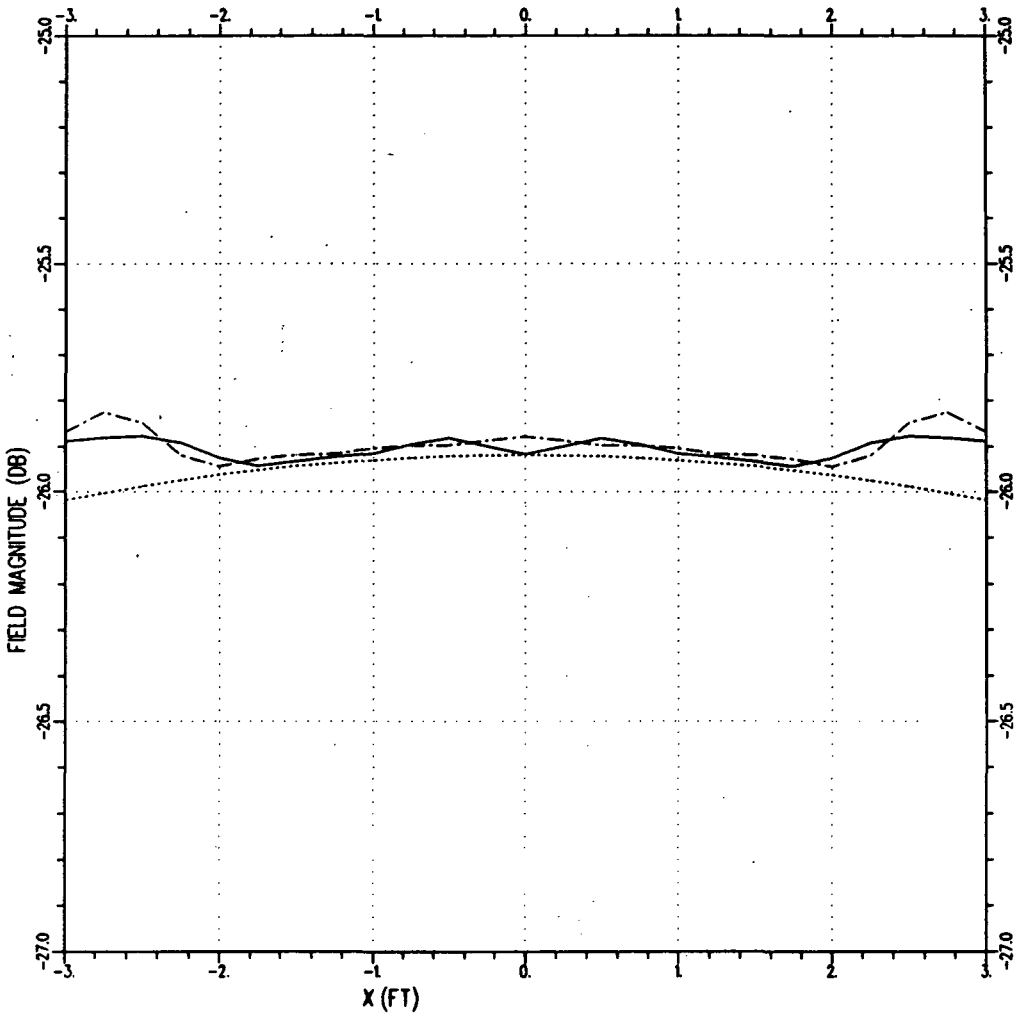

Figure 28(c): **Total PO field along the $y = 6.5ft$ cut after first- and second-order endpoint correction.**

Total PO after first- and second-order endpoint correction ————————

Total PO after first- and approximate second-order endpoint correction ·—·—·—·—·—·

GO ·····

y-component shown.

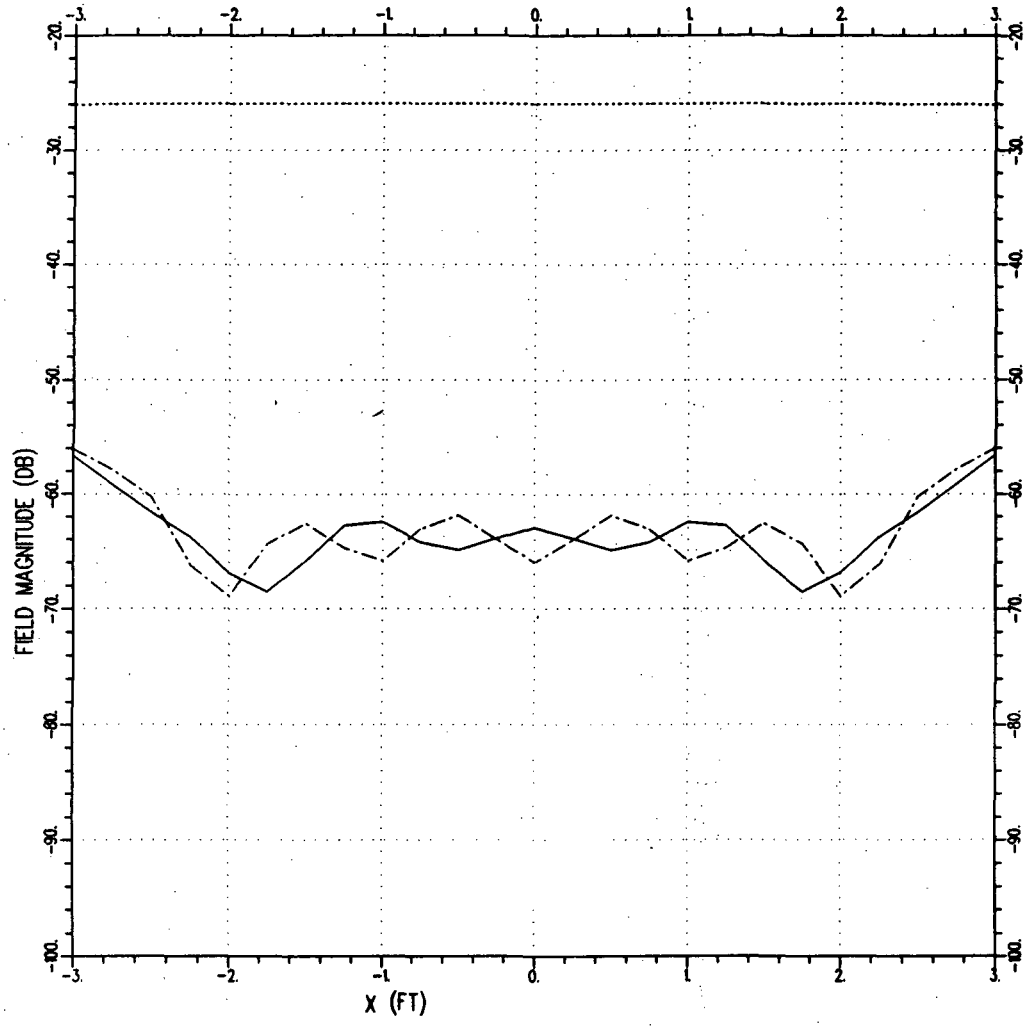

Figure 28(d): **Higher-order scattered fields along the $y = 6.5ft$ cut.**

Higher-order scattered fields ——————

Higher-order scattered fields using first- and approximate second-order endpoint correction —·—·—·—·—

GO ·····

y-component shown.

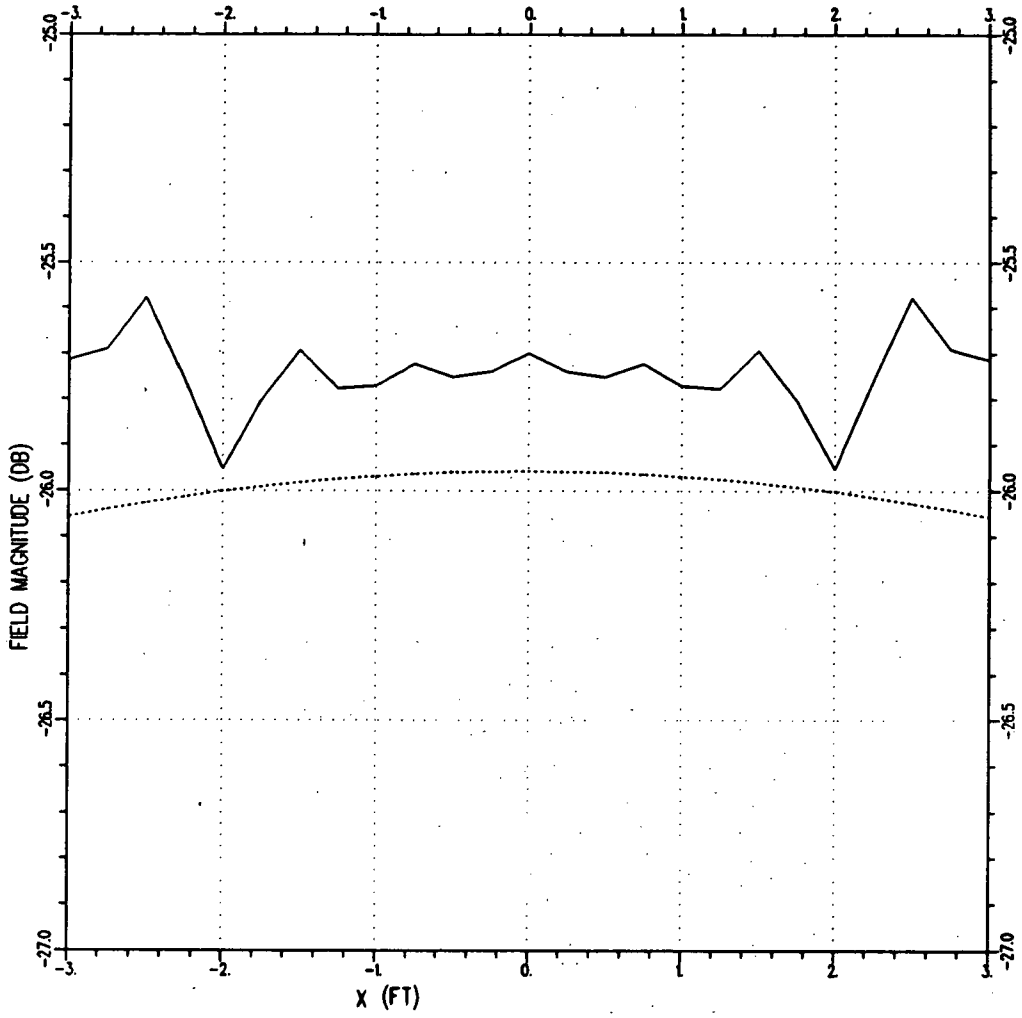

Figure 29(a): Total PO and GO fields along the $y = 8.294ft$ cut.
Total PO ————
GO .....
y-component shown.

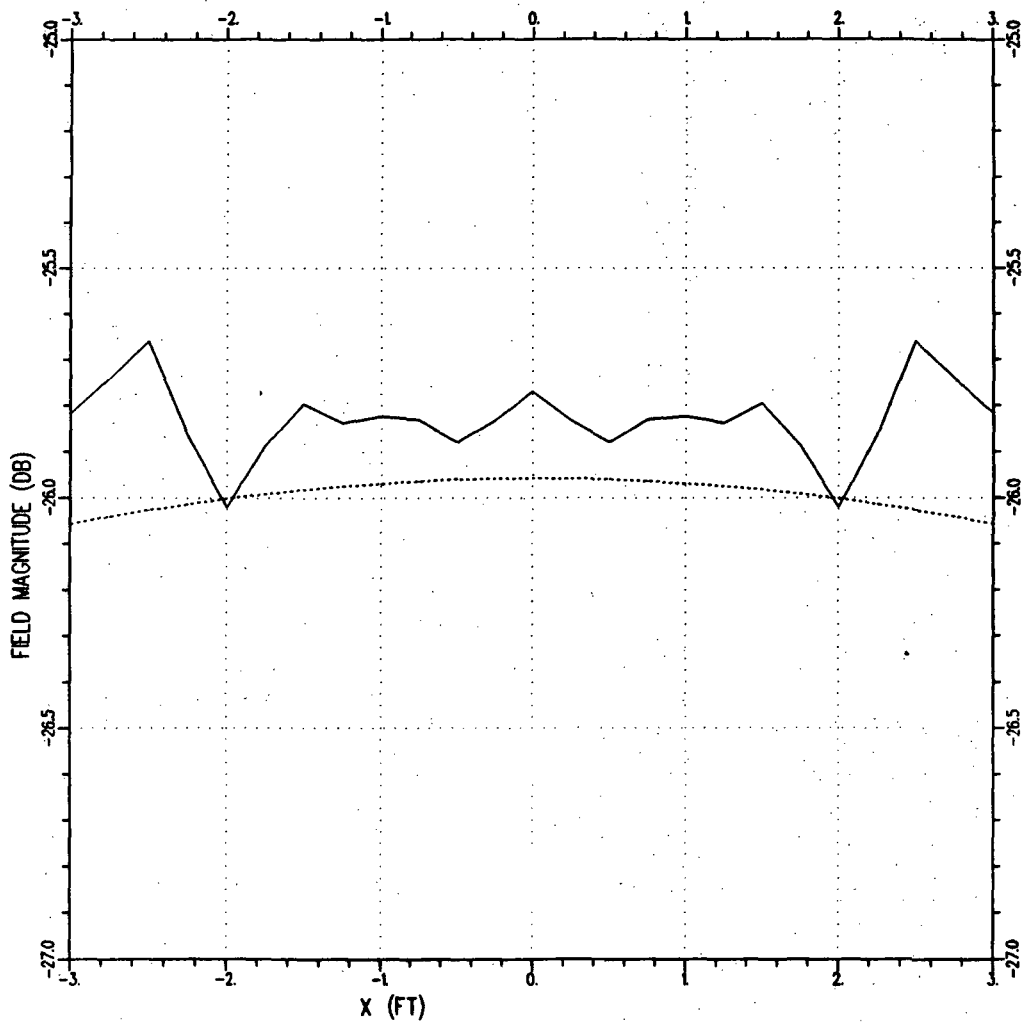

Figure 29(b): Total PO field along the $y = 8.294ft$ cut after first-order endpoint correction.

Total PO field after first-order endpoint correction. ————————

GO ····· ····· ····· ·····

y-component shown.

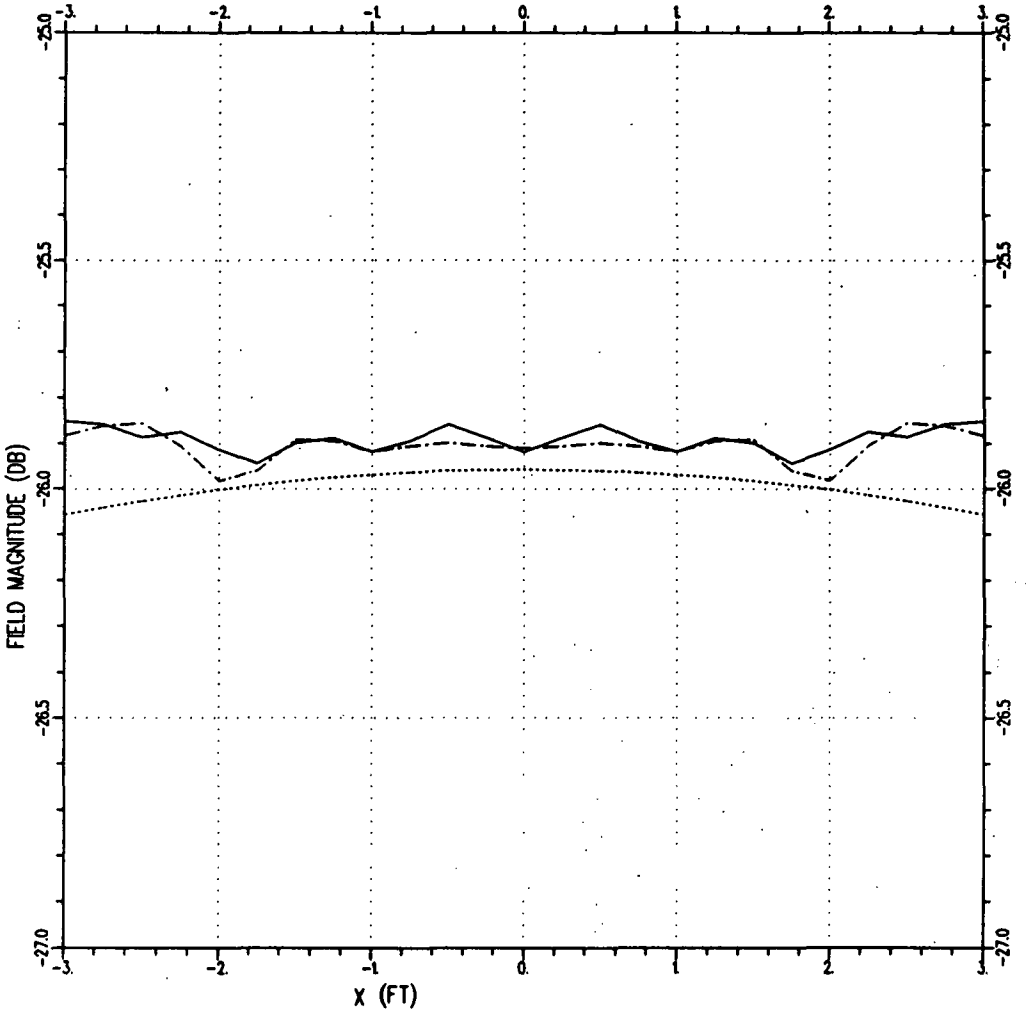

Figure 29(c): Total PO field along the $y = 8.294ft$ cut after first- and second-order endpoint correction.

Total PO after first- and second-order endpoint correction ——————

Total PO after first- and approximate second-order endpoint correction -·-·-·-·-·-

GO ·····

y-component shown.

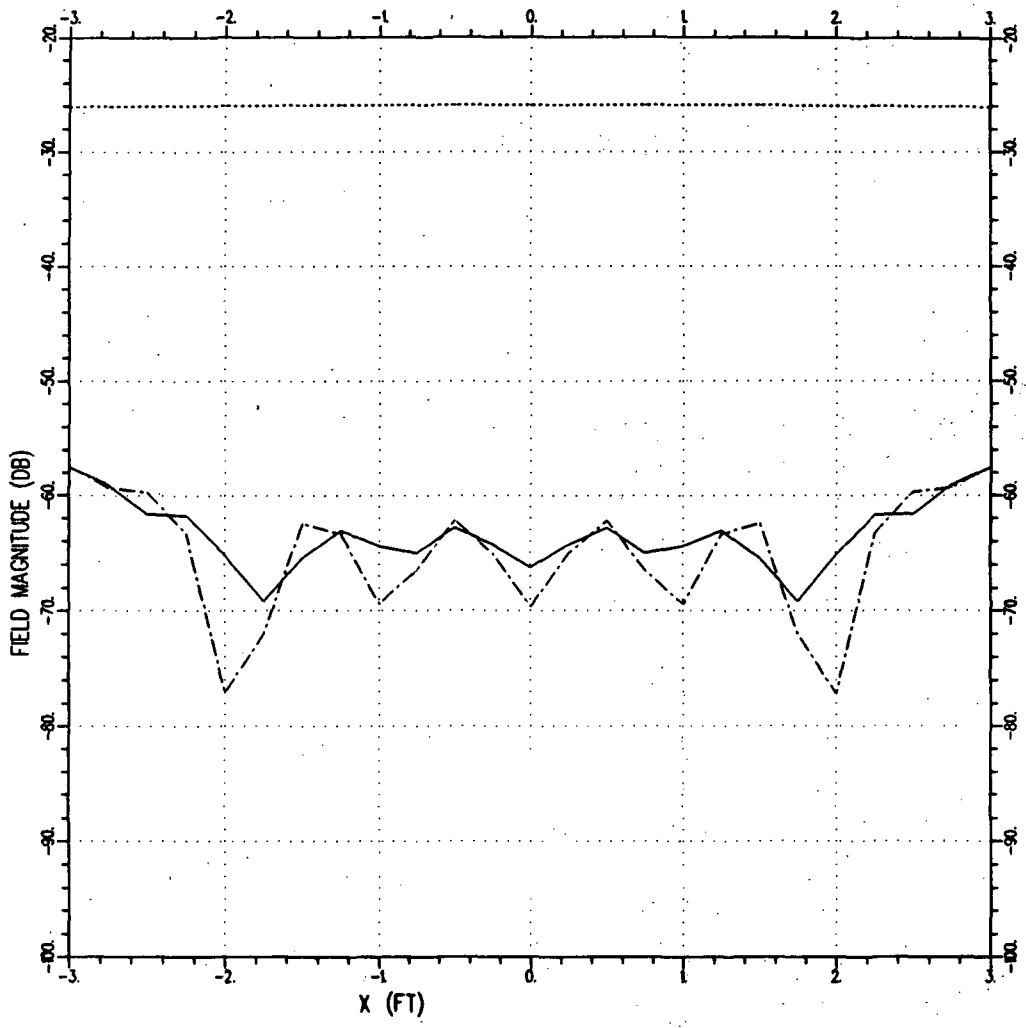

Figure 29(d): Higher-order scattered fields along the $y = 8.294ft$ cut.

Higher-order scattered fields ——————

Higher-order scattered fields using first- and approximate second-order endpoint correction ——·——·——

GO ·····

y-component shown.